Neuron, Vol. 37, 383–401, February 6, 2003, Copyright ©2003 by Cell Press

SCA7 Knockin Mice Model Human SCA7 and Reveal Gradual Accumulation of Mutant Ataxin-7 in Neurons and Abnormalities in Short-Term Plasticity

Seung-Yun Yoo,[1] Mark E. Pennesi,[1,2] Edwin J. Weeber,[1] Bisong Xu,[3] Richard Atkinson,[5] Shiming Chen,[7] Dawna L. Armstrong,[3] Samuel M. Wu,[1,2] J. David Sweatt,[1] and Huda Y. Zoghbi[1,4,5,6,*]

[1]Division of Neuroscience
[2]Department of Ophthalmology
[3]Department of Pathology
[4]Department of Pediatrics
[5]Department of Molecular and Human Genetics
[6]Howard Hughes Medical Institute
Baylor College of Medicine
Houston, Texas 77030
[7]Department of Ophthalmology and Visual Sciences
Department of Molecular Biology and Pharmacology
Washington University School of Medicine
St. Louis, Missouri 63110

Summary

We targeted 266 CAG repeats (a number that causes infantile-onset disease) into the mouse *Sca7* locus to generate an authentic model of spinocerebellar ataxia type 7 (SCA7). These mice reproduced features of infantile SCA7 (ataxia, visual impairments, and premature death) and showed impaired short-term synaptic potentiation; downregulation of photoreceptor-specific genes, despite apparently normal CRX activity, led to shortening of photoreceptor outer segments. Wild-type ataxin-7 was barely detectable, as was mutant ataxin-7 in young animals; with increasing age, however, ataxin-7 staining became more pronounced. Neurons that appeared most vulnerable had relatively high levels of mutant ataxin-7; it is interesting, however, that marked dysfunction occurred in these neurons weeks prior to the appearance of nuclear inclusions. These data demonstrate that glutamine expansion stabilizes mutant ataxin-7, provide an explanation for selective neuronal vulnerability, and show that mutant ataxin-7 impairs posttetanic potentiation (PTP).

Introduction

SCA7 is one of a growing number of autosomal dominant neurodegenerative diseases caused by the expansion of a translated CAG repeat. This repeat produces an abnormally long polyglutamine (Q) tract in the respective proteins and confers a toxic gain-of-function. Numbered among the nine polyglutamine diseases that have been identified so far are Huntington's disease and several of the spinocerebellar ataxias (SCAs) (Zoghbi and Orr, 2000; Nakamura et al., 2001). Like other SCAs, SCA7 causes progressive loss of motor coordination (ataxia), speech impairment (dysarthria), and swallowing difficulties (dysphagia), with longer CAG tracts producing more severe and rapid disease course. In distinction from the other polyglutaminopathies, however, SCA7 patients suffer from cone-rod dystrophy, which presents initially as loss of color discrimination in tritan axis (blue-yellow) followed by progressive pigmentary macular degeneration and loss of visual acuity, eventually leading to blindness (Neetens et al., 1990). Although SCA7 patients may present with either ataxia or visual loss, those with ≥59 repeats tend to develop visual impairment before the ataxia (Johansson et al., 1998). Extremely long CAG repeat tracts produce juvenile- or even infantile-onset disease, which is characterized by more rapid progression and a broader spectrum of phenotypes than adult-onset disease. It is worthy of note that the SCA7 protein, ataxin-7, is widely expressed throughout the brain and other tissues (Cancel et al., 2000; Lindenberg et al., 2000), yet only certain neuronal groups are vulnerable to its toxic effects. Only when the polyglutamine tract becomes sufficiently long does it cause more widespread damage.

Several groups have generated SCA7 transgenic mice using heterologous promoters (Yvert et al., 2000, 2001; La Spada et al., 2001). Yvert et al. (2002) generated two models expressing *SCA7* cDNA with 90 CAG repeats in either cerebellar Purkinje cells or rod photoreceptors. Both models showed degeneration of cell types that overexpress the transgene, and the authors also reported that mutant ataxin-7 is truncated to form an amino-terminal fragment (Yvert et al., 2000). More recently, the same group produced another two lines of mice expressing 10 or 128 CAG repeats in neurons using platelet-derived growth factor chain B promoter (Yvert et al., 2001). The mRNA levels of the transgene are the same in both of these lines, but they could detect no wild-type ataxin-7, which suggests that this protein is rapidly degraded (Yvert et al., 2001). La Spada et al. (2001) generated SCA7 mice expressing 92 CAG repeats using the murine prion protein promoter; these mice have retinal (La Spada et al., 2001) and cerebellar degeneration (Garden et al., 2002). This group found that cone-rod homeobox protein (CRX) interacts with ataxin-7 and suggested that CRX dysfunction is responsible for cone-rod dystrophy in SCA7 (La Spada et al., 2001). Although these studies nicely demonstrated that retinal and Purkinje cells are vulnerable to ataxin-7 toxicity in mice, there are important aspects of SCA7 pathogenesis that cannot be addressed with transgenic mouse models. Because heterologous promoters are used, transgenics cannot authentically reproduce the selective neuronal vulnerability that typifies SCA7. It is also difficult to determine whether the pathogenic events in these mice parallel those occurring in humans, or whether they might be in part due to transgene overexpression.

We wished to create a knockin mouse model that would express ataxin-7 at endogenous levels in the proper spatio-temporal pattern so that we could better address such open questions as selective neuronal vulnerability and the series of pathogenic events causing disease progression. The challenge with polyglutamine diseases is that the short life span of the mouse is limiting; prolonged exposure to the mutant protein is nor-

*Correspondence: hzoghbi@bcm.tmc.edu

mally necessary for neurons to develop dysfunction. There are two exceptions to this requirement, however: overexpression of the mutant (or even the wild-type) protein at high enough levels will produce neurodegeneration, as will extremely long CAG tracts (Fernandez-Funez et al., 2000; Gusella and MacDonald, 2000; Lin et al., 2001; Zoghbi and Botas, 2002). We were recently successful in generating a knockin mouse model of SCA1, another polyglutamine disease, using a very long polyglutamine tract (~154 CAGs) (Watase et al., 2002), but the fact that this repeat size has never been observed in a human SCA1 patient precluded direct comparisons between mouse and human. In the case of SCA7, on the other hand, extremely long repeats do occur (there are infantile SCA7 cases with 200–460 CAG repeats [Benton et al., 1998; Johansson et al., 1998; van de Warrenburg et al., 2001]), and this presented a unique opportunity. We reasoned that targeting a repeat in this size range would produce a mouse model that could be evaluated in direct comparison to infantile SCA7. To this end, we introduced 266 CAG repeats into the mouse *Sca7* locus (Sca7$^{266Q/5Q}$ mice).

Here we report the full characterization of Sca7$^{266Q/5Q}$ mice and show that these mice did indeed reproduce the salient features of infantile SCA7. These mice allowed us to probe important aspects of SCA7 pathogenesis such as selective neuronal vulnerability and the functional consequences of the mutant protein on the retina, cerebellum, and hippocampus without the confounding effects of overexpression. Lastly, certain intriguing differences between the knockin mice and previous transgenic models shed light on the strengths and limitations of each.

Results

Generation of Sca7$^{266Q/5Q}$ Mice

Mouse *Sca7* is highly homologous to human *SCA7*, with the peptide sequence showing 88.7% identity (Ström et al., 2002). Whereas the CAG repeat tract in human *SCA7* is polymorphic (ten repeats are the most common), mouse *Sca7* has only five CAG repeats in the corresponding region. We introduced 266 CAG repeats into the mouse *Sca7* locus using homologous recombination in embryonic stem (ES) cells (Figure 1A and see Experimental Procedures). Germline transmission of a targeted allele was confirmed by Southern analysis (Figure 1B) and PCR amplification of CAG repeats (data not shown).

Both mouse and human ataxin-7 have a nuclear localization signal (NLS) (David et al., 1997; Ström et al., 2002). In order to determine the subcellular localization of ataxin-7 in mouse cerebellum, we isolated the nuclear and cytoplasmic fractions and analyzed them by Western blotting (Figure 1C). Wild-type ataxin-7 was detected as 93 kDa protein in the nuclear extracts, but not in the cytoplasmic extracts of wild-type or Sca7$^{266Q/5Q}$ mice, showing that it is predominantly a nuclear protein in the cerebellum (Figure 1C). Mutant ataxin-7 is predicted to migrate at ≥190 kDa, given the size of expanded polyglutamine tract, but no immunoreactivity in this size range was detected in Sca7$^{266Q/5Q}$ lanes. Ataxin-7 immunoreactivity was detected in the stacking gel of the Sca7$^{266Q/5Q}$ nuclear extract lane (Figure 1C), suggesting that the mutant protein may exist in an insoluble form or in complexes with other proteins.

Table 1. Comparison between an Infantile SCA7 Patient and Sca7$^{266Q/5Q}$ Mice

Symptoms	Infantile SCA7 Patient	Sca7$^{266Q/5Q}$ Mice
Age of onset	1 month	5 weeks
Weight loss	✓	✓
Ptosis	✓	✓
Visual impairment	✓	✓
Ataxia	✓	✓
Muscle wasting	✓	✓
Kyphosis	✓	✓
Tremors	✓	✓
Death	6 months	4–5 months

Symptoms of an infantile SCA7 patient are compared with those of Sca7$^{266Q/5Q}$ mice. This patient is an individual IV-2 from BASCA kindred (Benton et al., 1998), and expanded CAG repeats from this patient were used to construct a targeting vector (see Experimental Procedures). ✓marks each symptom manifested in patient and Sca7$^{266Q/5Q}$ mice.

General Features of Sca7$^{266Q/5Q}$ Mice

We generated two independent lines of Sca7$^{266Q/5Q}$ mice (lines C1 and H10). Both lines were indistinguishable from wild-type littermates by visual observation until 5 weeks of age, at which time they started to develop features of infantile SCA7 patients, such as progressive weight loss, droopy eyelids (ptosis), ataxia, muscle wasting, curvature of the spine (kyphosis), and tremors (Table 1; Figure 1D). CAG repeat size in these two lines of Sca7$^{266Q/5Q}$ mice was relatively stable, occasionally showing less than ten CAG repeat (30 nucleotides) contraction, which did not change the progression or severity of the disease. Sca7$^{266Q/5Q}$ mice showed a similar weight gain pattern as wild-type mice up to 5 weeks but gained little if any weight afterward (Figure 1E). At the terminal stage of the disease, animals became extremely hypokinetic and did not drink nor eat, even when their chow was wetted and placed at the bottom of the cage. Sca7$^{266Q/5Q}$ mice died around 14–19 weeks of age.

Male Sca7$^{266Q/5Q}$ mice had reduced fertility after 13 weeks of age. Female Sca7$^{266Q/5Q}$ mice, on the other hand, failed to deliver pups when they were mated after 8 weeks of age. Some Sca7$^{266Q/5Q}$ mice developed myoclonic seizures around 12 weeks of age. Homozygous mice (Sca7$^{266Q/266Q}$ mice) showed a gene dosage effect, with their phenotype being more severe and disease progression more rapid, resulting in death around 7–8 weeks of age. The enhanced toxicity in the homozygous mice is most likely due to higher levels of expanded ataxin-7 (gain-of-function) rather than partial deficiency of wild-type ataxin-7's function: mice compound heterozygotes for expanded and a loss-of-function *Sca7* alleles (Sca7$^{266Q/-}$ mice) do not show enhanced toxicity as those homozygotes for the expanded allele (S.-Y.Y. and H.Y.Z, unpublished data). Because Sca7$^{266Q/266Q}$ mice were so severely affected and because both knockin lines showed similar phenotypes, only Sca7$^{266Q/5Q}$ mice (line H10) were used for subsequent characterization.

Cone-Rod Dystrophy in Sca7$^{266Q/5Q}$ Mice

Sca7$^{266Q/5Q}$ mice were born with normal eyes, but as they aged, the eyes receded and ptosis developed. In order

to determine whether this was accompanied by a progressive decline of retinal function, we evaluated electroretinograms (ERGs) of wild-type and Sca7$^{266Q/5Q}$ mice at three different ages: 5, 9, and 14 weeks. The ERGs of wild-type mice from these age groups were not significantly different, so we pooled the data for all wild-type animals. We measured scotopic b-waves, a-waves, and cone-driven b-waves (Table 2; Figure 2)

The scotopic (dark-adapted) b-wave is an extracellular field potential that arises primarily from ON-rod bipolar cells in response to dim flashes of light (Pugh et al., 1998). The relationship between scotopic b-wave amplitude and intensity can be modeled using a hyperbolic saturation function (see Experimental Procedures). This model yields two parameters, $b_{max,scot}$ and $I_{0.5}$, representing the maximum b-wave amplitude and the intensity that provides half saturation, respectively. At 5 weeks of age, scotopic b-waves from Sca7$^{266Q/5Q}$ mice were indistinguishable from their wild-type counterparts. However, as they aged, Sca7$^{266Q/5Q}$ mice demonstrated both a decline in $b_{max,scot}$ and an increase in $I_{0.5}$ (Table 2). At 9 weeks, rod-driven function had decreased to 65% compared to wild-type. By 14 weeks, $b_{max,scot}$ had decreased to 25% of wild-type (Figures 2A–2D). It was not possible to study the mutant mice beyond 15 weeks because of their frailty. Our data suggest that the rod system of Sca7$^{266Q/5Q}$ mice develops properly and is capable of normal phototransduction. The decrease in the scotopic b-wave may have resulted from a defect in the rod bipolar cells, from decreased input of the rod photoreceptors, or both.

To examine rod photoreceptor function, we analyzed the ERG a-wave, which arises almost exclusively from the rod photoreceptors in mouse (Pugh et al., 1998). An intense flash was used to measure the saturated a-wave amplitude, a_{max} (Figures 2E–2H). At 5 weeks of age, there was no significant difference between the wild-type and Sca7$^{266Q/5Q}$ mice. Sca7$^{266Q/5Q}$ mice showed a steady decline in saturated a-wave amplitude with age: at 9 weeks, a_{max} had declined to 60%, and by 14 weeks, a_{max} was decreased to 30% of normal. To analyze the amplification of the rod transduction cascade, a series of a-waves were fitted to Equation 1 (see Experimental Procedures) (Lamb and Pugh, 1992), and the parameter *kA* was derived (Figures 2I–2L). There was no statistically significant difference in the amplification parameter *kA* between wild-type and Sca7$^{266Q/5Q}$ mice at any of the ages tested (Table 2). The amplitude of the a-wave is directly proportional to the number of cyclic nucleotide-gated channels that close in response to light (Pugh et al., 1998). Thus, the decrease of the a-wave in Sca7$^{266Q/5Q}$ mice provides direct evidence for a rod photoreceptor defect. The normal amplification constant suggests that this deficit is not due to a change in the relative enzymatic activities of the proteins involved in the transduction cascade. A loss of photoreceptors or decrease in the photoreceptor outer segment length could diminish the a-wave amplitude without necessarily changing the amplification constant. To determine whether the dysfunction extended to cones, we used the double flash technique to isolate responses from cone photoreceptors (Lyubarsky et al., 1999). Figures 2M–2P show the ERG response to a white flash, which stimulates both S and M cones. To establish whether there was any functional difference between S and M cones, we filtered the light using band pass filters specific for the two classes of cones and measured the response (Figures 2Q–2T and 2U–2X). At 5 weeks, wild-type and Sca7$^{266Q/5Q}$ mice showed little difference when stimulated with white or UV light, but stimulation with green light revealed a statistically significant decrease ($p = 0.039$) (Table 2; Figure 2V). The cone response continued to decrease at 9 weeks, and by 14 weeks, it was undetectable (Figures 2P, 2T, and 2X). The trend toward a decline at 5 weeks and the significant decline at 9 weeks of cone ERGs suggests that cone dysfunction occurs prior to rod dysfunction in Sca7$^{266Q/5Q}$ mice.

The abnormal ERG results prompted us to look at the expression levels of several photoreceptor-specific genes in the eyes of Sca7$^{266Q/5Q}$ mice (Figure 3A). We decided to look at the expression levels of three photopigment genes (blue cone opsin [*Bcp*], green cone opsin [*Gcp*], and rhodopsin [*Rho*]), rod transducin (*Gnat1*), and rhodopsin kinase (*Rhok*). *Bcp* (*S opsin*) and *Gcp* (*M opsin*) are cone-specific markers, whereas *Rho* and *Gnat1* are rod-specific markers. *Rhok* is present in both cones and rods (Lyubarsky et al., 2000). Expression of all these genes showed a progressive decrease with age. Cone-specific markers showed about 60% reduction in a presymptomatic 4-week-old mutant (Figure 3A). The youngest mice that were tested on ERGs were 5 weeks old when they began to show some decrease in cone activity (Table 2; Figure 2). It is interesting to note that the cone photoreceptors remained functional even with more than 60% decrease of both cone-specific photopigments. Rod-specific markers were downregulated later than cone-specific markers. This may explain why cone dysfunction appeared earlier than rod dysfunction in ERG studies.

Hematoxylin and eosin staining of Sca7$^{266Q/5Q}$ retinas revealed progressive shortening of outer segments and thinning of inner plexiform layer (IPL) (Figure 3B). Although endogenous levels of ataxin-7 were very low in wild-type retina, mutant ataxin-7 accumulated in Sca7$^{266Q/5Q}$ retina, forming microaggregates around 8 weeks of age (Table 3)—and single, large nuclear inclusions (NIs) around 10 weeks (Figures 3C and 4A)—when retinal dysfunction has already set in. Mutant ataxin-7 accumulation was observed throughout the retina, but it occurred more rapidly in outer nuclear layer (ONL) (specifically the top layer of ONL) and inner nuclear layer (INL) than in ganglion cell layer (GCL) (Figures 3C and 4A). In mature mouse retina, the nuclei of cones are aligned directly beneath the inner segments, i.e., in the top layer of ONL (Carter-Dawson and LaVail, 1979; Rich et al., 1997). To verify that the nuclei harboring mutant ataxin-7 signals in the ONL of 10-week-old Sca7$^{266Q/5Q}$ retina are those of cones, we double-labeled retina sections with ataxin-7 antibody (1261) in combination with neuron-specific enolase (NSE) antibody, which labels cones (Rich et al., 1997). All ataxin-7-positive nuclei in ONL, at this age, turned out to be those of cones, suggesting that accumulation of mutant ataxin-7 starts in the cones in the ONL (Figure 4B). We also performed double labeling using 1261 antibody in combination with either calbindin antibody (a marker for horizontal cells and amacrine cells) or protein kinase C (PKC) antibody (a marker for bipolar cells) on 10-, 12-, and 15-week-

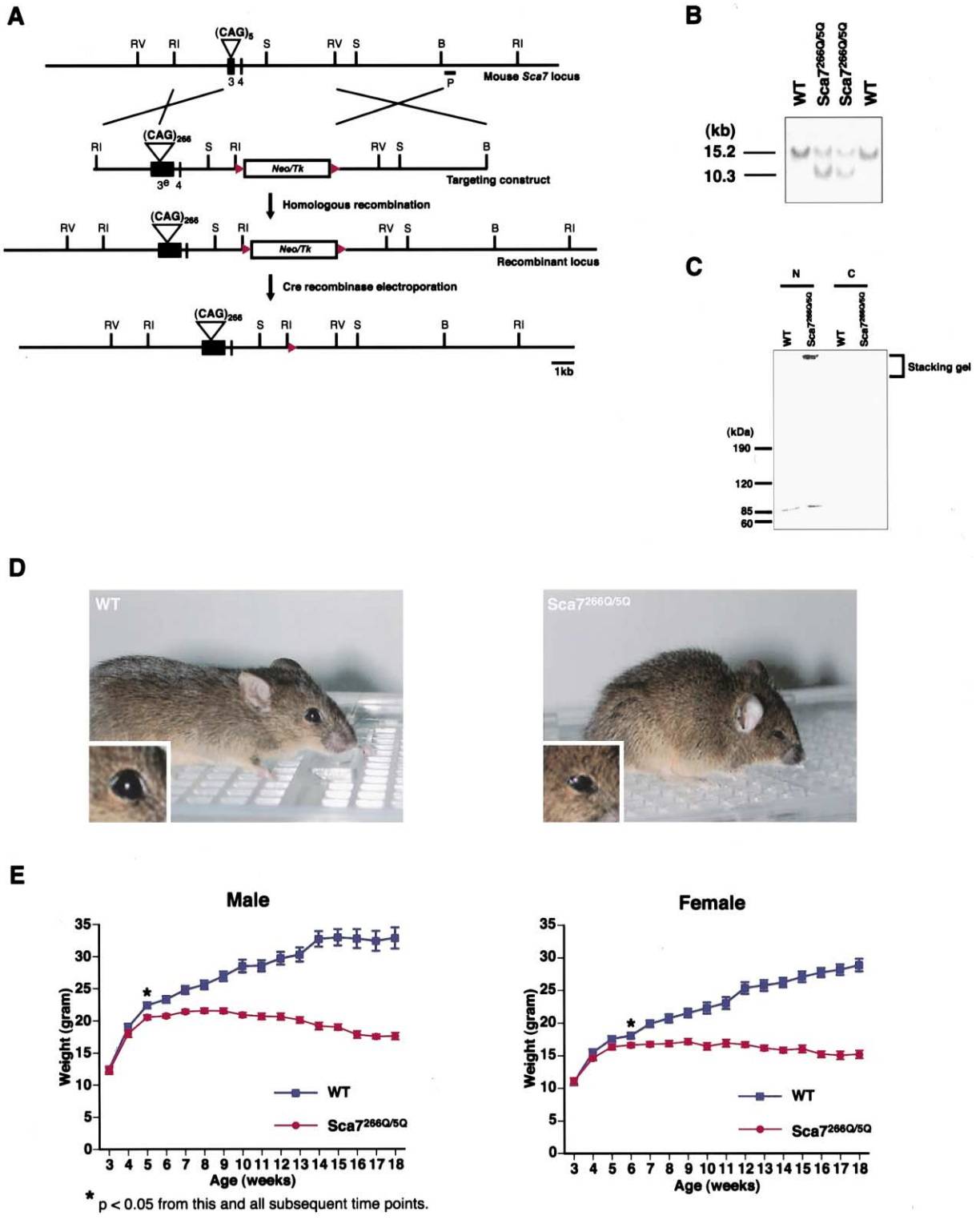

Figure 1. Generating Sca7$^{266Q/5Q}$ Mice

(A) Targeting scheme. The top diagram shows a simplified version of mouse *Sca7* locus near exons 3 and 4. Targeting construct introduced 266 CAG repeats (inverted triangle) and flanking regions from human *SCA7* into exon 3, obtaining a targeting frequency of 4%. Electroporation of Cre recombinase into the positive ES clones allowed the excision of the *Neomycin* (*Neo*)/*Thymidine kinase* (*Tk*) selection cassette (shown as an open box) from the targeted locus. P indicates a probe used for Southern analysis. Red arrowheads indicate *lox*P sites. Abbreviations are as follows: 3, exon 3; 4, exon 4; 3^e, engineered exon 3 with 266 CAG repeats; RV, EcoRV; RI, EcoRI; S, ScaI; and B, BamHI.

(B) Germline transmission of a targeted allele. Southern analysis of EcoRI-digested tail DNA revealed 15.2 kb wild-type and 10.3 kb mutant bands in Sca7$^{266Q/5Q}$ mice. Only the 15.2 kb band was detected from wild-type (WT) mice.

(C) Ataxin-7 is predominantly nuclear in the cerebellum, and expanded ataxin-7 is expressed in vivo. Both wild-type and mutant

old retina sections (Figure 4C and data not shown) and confirmed that the mutant protein accumulated in nuclei of all three interneurons in INL.

Although NIs were present in all three nuclear layers in the retina, apoptosis was observed only in ONL (Figure 4D). More importantly, retinal dysfunction occurred prior to the loss of photoreceptors: both rod and cone activities were significantly reduced at 9 weeks (Figure 2), but only few photoreceptors were TUNEL positive in ONL of 10-week-old Sca7$^{266Q/5Q}$ mice (Figure 4D). To quantify the loss of photoreceptors, we counted the number of nuclei in the vertical length of ONL (see Experimental Procedures) at 15 weeks of age. Sca7$^{266Q/5Q}$ mice lost about 20% of photoreceptors in the ONL at this age (WT, 10.9 $\pm$ 0.1; Sca7$^{266Q/5Q}$, 8.8 $\pm$ 0.11; $p < 0.0001$). We also observed progressive activation of Müller glia in Sca7 $^{266Q/5Q}$ retina, which is a good indicator for photoreceptor degeneration (Semple-Rowland et al., 1991; de Raad et al., 1996; Hong et al., 2000; Rattner et al., 2001) (Figure 4E). Our results indicate that the abnormal ERGs in Sca7$^{266Q/5Q}$ mice are not due to the loss of photoreceptors, but to photoreceptor dysfunction and transcriptional dysregulation of photoreceptor-specific genes.

CRX Dysfunction in SCA7 Revisited

La Spada et al. recently observed that CRX interacts with ataxin-7, and proposed that mutant ataxin-7 interference with CRX function causes the cone-rod dystrophy in SCA7 (La Spada et al., 2001). In agreement with previous work on SCA7 transgenic mice, CRX-regulated photoreceptor-specific genes such as *Bcp*, *Gcp*, *Rho*, and *Gnat1* were downregulated in Sca7$^{266Q/5Q}$ mice. But *Rhok*, which is not altered in *Crx*-deficient mice (Furukawa et al., 1999), was also progressively downregulated in Sca7$^{266Q/5Q}$ mice (Figure 3A). Furthermore, we found that CRX protein levels did not change up to 14 weeks of age in Sca7$^{266Q/5Q}$ retina (Figure 5A). Electrophoretic mobility shift assays (EMSAs) showed that CRX binding to Ret-4, a well-characterized CRX-responsive element in the bovine rhodopsin promoter (Chen and Zack, 1996), was the same as wild-type in 3- to 7-, 10-, and 12-week-old Sca7$^{266Q/5Q}$ retina (Figure 5B and data not shown). To further probe the role of CRX dysfunction in Sca7$^{266Q/5Q}$ mice, we analyzed the expression levels of additional genes that are not altered (*Rom1* and *Rbp3*) as well as a gene that is upregulated (*Cnga3*) in *Crx*$^{-/-}$ mice based on Northern analyses (Furukawa et al., 1999) (Figure 5C). *Rom1* encodes retinal outer segment membrane protein 1 (Rom1), which is a structural component of rod photoreceptor outer segments (Goldberg and Molday, 1996), and *Rbp3* encodes interphotoreceptor retinal binding protein (IRBP). *Cnga3* encodes cGMP-gated cone channel. All these genes were progressively downregulated in Sca7$^{266Q/5Q}$ mice in contrast with *Crx* null mice where they were either upregulated or unaltered (Figures 5C and 5D). These results suggest that CRX dysfunction might not be the primary and/or sole mediator of cone-rod dystrophy in SCA7. Transcriptional dysregulation in Sca7$^{266Q/5Q}$ retina might arise from more global repression of photoreceptor-specific genes.

Cerebellar Dysfunction in Sca7$^{266Q/5Q}$ Mice

In addition to the retina, the cerebellum is one of the most commonly affected tissues in infantile SCA7. Sca7$^{266Q/5Q}$ mice manifested motor incoordination on the rotarod by 5 weeks. Although their rotarod performance improved with training, they did not last as long on the rotarod as their wild-type littermates (Figure 6A). By 8–9 weeks, gait ataxia was apparent and motor coordination deteriorated further. Mutant mice soon became kyphotic, then hypoactive at the terminal stage of disease. Pathologic inspection of Sca7$^{266Q/5Q}$ brain revealed that it was smaller than wild-type. TUNEL assays at 15 and 18 weeks detected no positive signals in cerebellum (data not shown). In order to evaluate whether there was any loss of Purkinje cells in Sca7$^{266Q/5Q}$ cerebellum at the terminal stage, we counted the number of Purkinje cells in a 5 μm section through the midsagittal cerebellar region at 18 weeks. No significant Purkinje cell loss was detected in the mutants (WT, 273.3 $\pm$ 5.8; Sca7$^{266Q/5Q}$, 264.3 $\pm$ 8.6; $p = 0.2$), which is consistent with the findings in some infantile SCA7 cases (Carpenter and Schumacher, 1966). Immunofluorescence confocal microscopy revealed that although the number of Purkinje cells and their dendritic arbors appeared normal in 16-week-old Sca7$^{266Q/5Q}$ cerebellum, the cell bodies were significantly smaller than those of wild-type Purkinje cells (Figures 6B and 6C).

Mutant Ataxin-7 Is Highly Insoluble and Gradually Accumulates in Neurons

No ataxin-7 immunostaining was apparent in wild-type brain sections with the 1261 antibody made against amino acid 1–19 of human ataxin-7 (kind gift of J.-L. Mandel [Lindenberg et al., 2000; Yvert et al., 2000]) and SCA7 (1-135) antibody made against amino acid 1–135 of mouse ataxin-7 (kind gift of M. Holmberg [Ström et al., 2002]) (Figure 7A and data not shown). The same antibodies were, however, able to detect mutant ataxin-7 in Sca7$^{266Q/5Q}$ brain, and the staining became denser as the animal aged (Table 3; Figure 7A). The pattern of immunoreactivity varied, however, in different neurons. NIs did appear in nonaffected areas (areas that are typically spared in infantile SCA7 patients [Havener, 1951; Carpenter and Schumacher, 1966]) first; however, they were in glial cells and not in neurons. Neurons of the retina and cerebellum, two areas whose functions are profoundly affected in infantile SCA7 patients and Sca7$^{266Q/5Q}$ mice, showed faster accumulation of mutant ataxin-7 than other areas of the brain in Sca7$^{266Q/5Q}$ mice. It is interesting that although mutant ataxin-7 accumulation increased over time, NIs were *not* formed until much

ataxin-7 are present only in the nuclear extracts of 7-week-old mice. Mutant ataxin-7 immunoreactivity is observed in the stacking gel. N and C are nuclear and cytoplasmic extracts, respectively.

(D) 16-week-old WT and Sca7$^{266Q/5Q}$ mice. At this age, mutant mice weigh only 50% of wild-type counterparts and are extremely hypoactive. Tremor is triggered whenever they initiate movement. Ptosis and kyphosis are apparent in mutant mouse shown here.

(E) Both male and female Sca7$^{266Q/5Q}$ mice show retarded growth after 5 weeks of age.

Table 2. Summary of ERG Parameters

Genotype	Age (weeks)	$b_{max,scot}$ (μV)	$I_{0.5}$ (scotopic cd-s/m^2)	a_{max} (μV)	kA s^{-2} (scotopic cd-s/m^2)$^{-1}$	$b_{max,phot}$ (μV)	b_{365nm} (μV)	b_{500nm} (μV)
Wild-type	5–14	625 ± 10 (n = 10)	(14.6 ± 1.3) × 10^{-4}	610 ± 145	3360 ± 1610 (n = 8)	185 ± 35 (n = 14)	125 ± 35	150 ± 40
Sca7$^{266Q/5Q}$	5	690 ± 9 (n = 4)	(15.7 ± 1.0) × 10^{-4}	650 ± 120	3750 ± 1200 (n = 4)	180 ± 40 (n = 7)	115 ± 20	120 ± 35
Sca7$^{266Q/5Q}$	9	360 ± 10 (n = 5)	(31.7 ± 3.2) × 10^{-4}	320 ± 50	3700 ± 1690 (n = 5)	75 ± 25 (n = 5)	35 ± 15	15 ± 10
Sca7$^{266Q/5Q}$	14	150 ± 4 (n = 8)	(55.1 ± 5.8) × 10^{-4}	165 ± 110	2800 ± 1670 (n = 5)	0 (n = 4)	0	0

The first column indicates the genotype of the mice. Mice were divided into three age groups: 5, 9, and 14 weeks. The parameter, $b_{max,scot}$, represents the saturating amplitude of the scotopic b-wave, and $I_{0.5}$ is the intensity, measured scotopic cd-s/m^2, which produces one-half of $b_{max,scot}$. These values were obtained by measuring the peak amplitude of filtered b-waves at increasing intensity and then fitting these values to a hyperbolic saturating function (Naka-Rushton). The value shown in the table represents the best fit, while the second number is the error of the fit. For the remaining parameters in the table, the first value represents the mean and the second value represents the standard error. The parameter, a_{max}, is the amplitude of the a-wave in response to an intense, saturating flash measured to produce 2.97 log scotopic cd-s/m^2. In a photoreceptor with a normal outer segment, this flash is estimated to produce 880,000 photoisomerizations/rod. The parameter *kA* was obtained by fitting the a-wave using the model developed by Lamb and Pugh. $b_{max,phot}$ measures the peak amplitude of the filtered b-wave in response to a flash that produces 143 photopic cd/m^2. The parameters b_{365nm} and b_{500nm} are the cone-isolated responses to these flashes, which produce 6,500 and 8,800 photoisomerizations/cone, respectively.

later in the disease course (10–12 weeks) in these two affected areas (Figures 3C, 4A, and 7A). This accumulation of mutant ataxin-7 was not due to the upregulation of mutant *Sca7* mRNA, since there was no difference between the level of mutant and wild-type *Sca7* mRNA in the mutant brain (Figure 7B).

The hippocampus was another area where accumulation of mutant ataxin-7 in neurons was occurring around the same time as the retina and cerebellum, which prompted us to search for functional impairments specific to this tissue (see below). It is noteworthy that in three areas that develop functional impairments in Sca7$^{266Q/5Q}$ mice (retina, cerebellum, and hippocampus), the aggregates became ubiquitin positive around 12 weeks (Table 3). Ubiquitin-positive NIs colocalized with Hsc70, and the number of ubiquitin- and Hsc70-positive NIs increased over time (data not shown). No CRX or TATA binding protein (TBP) immunoreactivity was observed in NIs of affected neurons up to 18 weeks (Table 3). NIs throughout the brain became CREB binding protein (CBP) positive around 18 weeks (Table 3).

Wild-type ataxin-7 was detected only in nuclear extracts, but not cytoplasmic extracts of wild-type and Sca7$^{266Q/5Q}$ cerebella (Figure 1D). We failed to detect any SDS-soluble mutant ataxin-7 or any evidence of truncated mutant ataxin-7 using N-terminal (1261) and C-terminal (1597) (Yvert et al., 2000) antibodies in the separating gel (Figure 1C and data not shown). Mutant ataxin-7 was detected only in the stacking gel, suggesting that this protein exists as an insoluble multimer or in complexes with other proteins. Another possibility is that the conformation of soluble mutant ataxin-7 differs from that of insoluble mutant ataxin-7, and the epitope of soluble mutant ataxin-7 is masked. We reasoned that because the mutant protein accumulated with age, we might be able to detect the soluble form in younger animals. Cerebellar nuclear extracts were prepared from 2-, 5-, 7-, 10-, 12-, and 15-week-old Sca7$^{266Q/5Q}$ mice, and Western blotting was performed using the 1261 antibody. Expression levels of wild-type ataxin-7 were very low in both wild-type and Sca7$^{266Q/5Q}$ mice, and mutant ataxin-7 immunoreactivity in the stacking part of the gel increased with age. Surprisingly, we were unable to detect the soluble mutant ataxin-7 even in 2-week-old mice when very faint immunoreactivity was found in the stacking gel. This suggests that there is little accumulation of mutant ataxin-7 at this age. These data indicate that even in 2-week-old Sca7$^{266Q/5Q}$ cerebellum, soluble mutant ataxin-7 might exist in a conformation that is not easily detectable with 1261 antibody or that it is still efficiently turned over. By 5 weeks, however, mutant ataxin-7 begins to accumulate, becoming part of insoluble complexes.

Selective Impairment of PTP

We investigated hippocampal function in Sca7$^{266Q/5Q}$ mice, since the hippocampus is another area in which mutant ataxin-7 rapidly accumulated in neurons (Table 3; Figure 8A). Occasional punctate nuclear immunostaining of ataxin-7 was observed in hippocampal CA1 pyramidal neurons around 12 weeks, and by 15 weeks, NIs became larger and dotted the entire hippocampus (Figure 8A and data not shown). We investigated

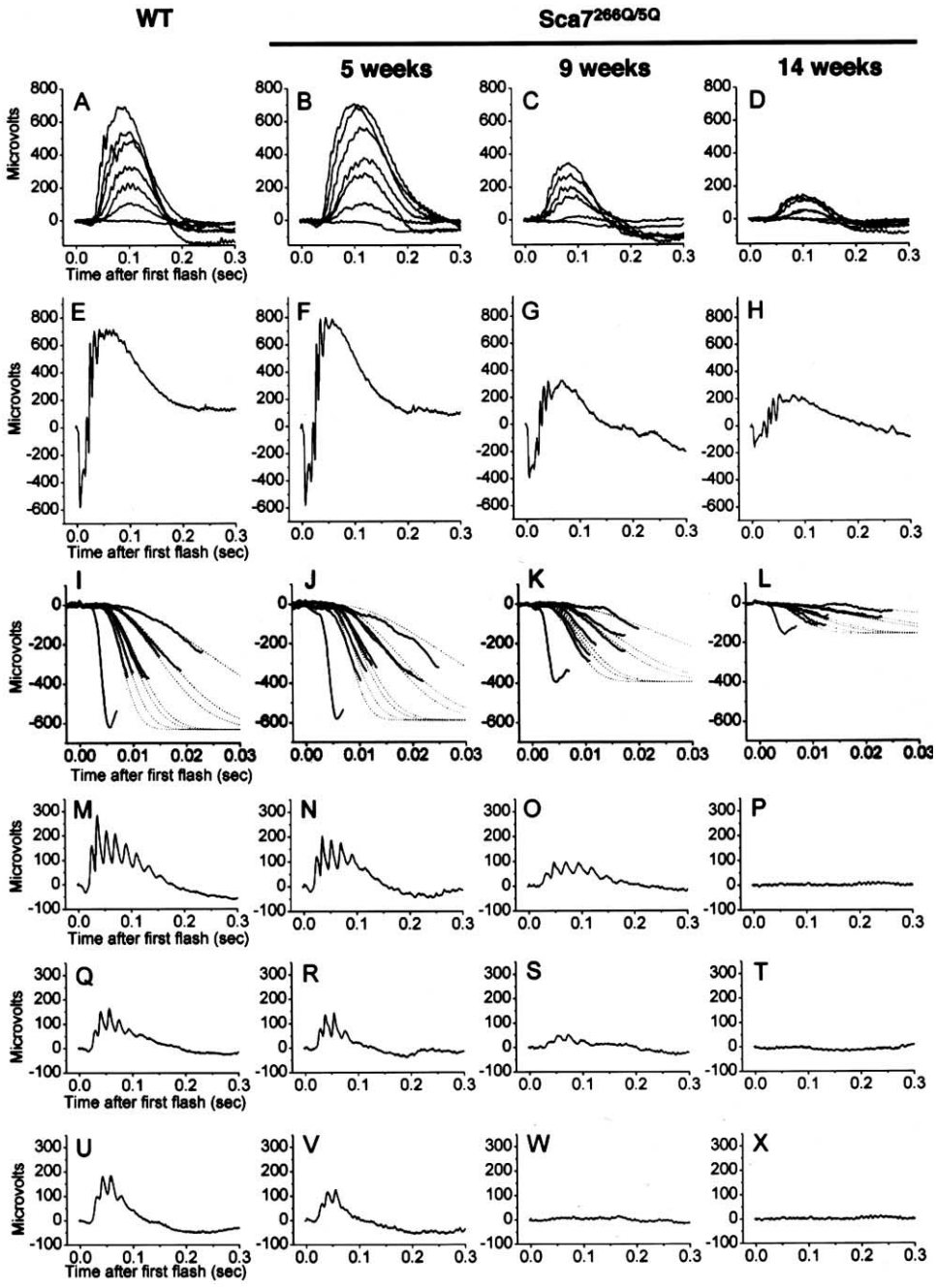

Figure 2. Representative ERGs from Wild-Type and Sca7$^{266Q/5Q}$ Mice

The first column contains data from wild-type mice, while subsequent columns show data from Sca7$^{266Q/5Q}$ mice at increasing ages.

(A–D) Measurement of the scotopic b-wave. Traces were obtained using a series of 500 nm flashes with intensities ranging from −3.86 to −1.76 log scotopic cd-s/m^2 (estimated to produce between 0.13 and 16.1 photoisomerizations/rod in photoreceptors with normal outer segments). Each trace represents the average of at least five flashes.

(E–H) ERG response to an intense flash (2.92 log scotopic cd-s/m^2 or an estimated 800,000 photoisomerizations/rod).

(I–L) a-wave response to flashes varying in intensity from −0.51 to 2.92 log scotopic cd-s/m^2 (290–800,000 photoisomerizations/rod). Traces have been fit using the Lamb-Pugh model, as described in Experimental Procedures.

(M–P) Cone isolated ERGs using the double flash method. Only the response to the second white flash is displayed. To distinguish between S cones and M cones, the second flash was filtered at 365 nm (Q–T) and 500 nm (U–X). M cones were affected before S cones. Progressive decreases in scotopic b-waves, a-waves, and cone-driven b-waves indicate retinal dysfunction in Sca7$^{266Q/5Q}$ mice.

whether synaptic physiology was altered at the time of mutant ataxin-7 accumulation in hippocampal area CA1. We prepared hippocampal slices from 12-week-old Sca7$^{266Q/5Q}$ mice and littermate controls and characterized synaptic transmission and short- and long-term plasticity using extracellular field recordings in stratum

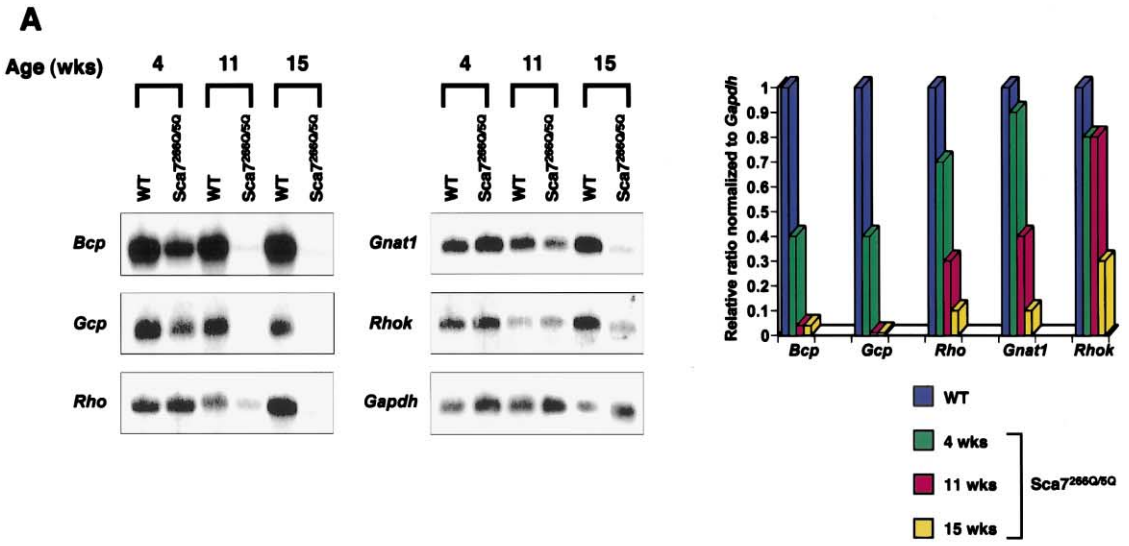

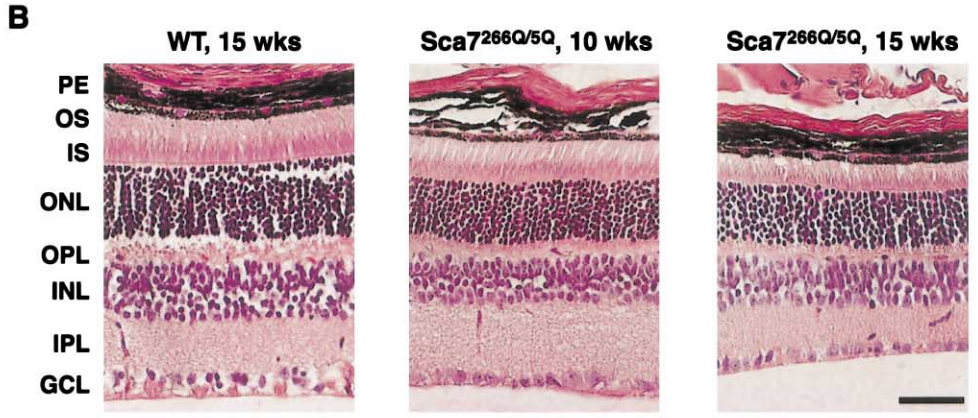

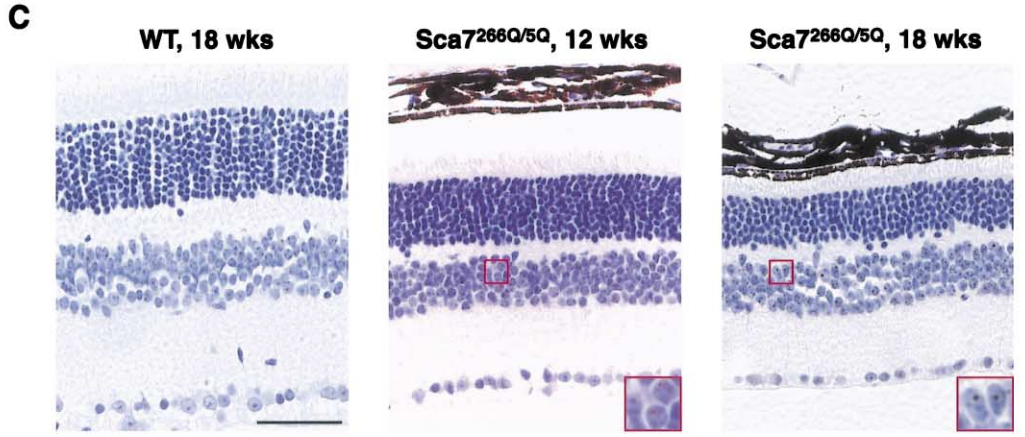

Figure 3. Retinal Degeneration in Sca7$^{266Q/5Q}$ Mice

(A) Progressive downregulation of photoreceptor-specific genes in Sca7$^{266Q/5Q}$ eyes. Expression levels of five photoreceptor-specific genes using total RNAs from WT and Sca7$^{266Q/5Q}$ mice show a progressive decrease with age. The expression of cone-specific genes (*Bcp* and *Gcp*) diminishes before the rod-specific genes (*Rho* and *Gnat1*) and decreases more rapidly with time. Signals from each lane were normalized to *Gapdh*, and ratios were calculated relative to that of the WT at each age.

(B) Shortening of the outer segment in Sca7$^{266Q/5Q}$ retina. The retinal layer thins with age, mainly due to the thinning of the IPL. At 10 weeks, the outer segments in mutant mice become more dispersed than WT. Shortening of the outer segments continues as mice age, and after 12 weeks, the outer segments are no longer detectable in Sca7$^{266Q/5Q}$ retina. Abbreviations for each retinal layer are as follows: PE, pigment epithelium; OS, outer segment; IS, inner segment; ONL, outer nuclear layer; OPL, outer plexiform layer; INL, inner nuclear layer; IPL, inner plexiform layer; and GCL, ganglion cell layer.

Table 3. Time-Dependent Appearance of NIs in the Brain and Retina

Area	NI[a] Appearance (Weeks)	Ub-Positive Staining (Weeks)	Hsc70-Positive Staining (Weeks)	CBP-Positive Staining (Weeks)	TBP-Positive Staining (Weeks)
Spinal cord[b]	≥5	≥12	≥12	≥18	-
Pons/Medulla[b]	≥5	≥12	≥12	≥18	-
Olfactory bulb[b]	≥7	≥15	≥15	≥18	-
Cortex[b]	≥5	≥12	≥15	≥18	-
Cerebellum	≥12	≥12	≥12	≥18	-
Hippocampus	≥13	≥13	≥13	≥18	-
Retina	≥8	≥12	≥12	-	-

[a] Here used to denote any visible aggregation, including microaggregates.
[b] In these tissues, NIs appeared in glial cells at the designated ages.

radiatum in area CA1. We detected no difference in baseline synaptic transmission, as input-output functions for increasing stimulus intensities in Sca7$^{266Q/5Q}$ mice are similar to wild-type (Figure 8B). Normal baseline synaptic transmission suggests that the synaptic connectivity in Sca7$^{266Q/5Q}$ mice is normal. Paired pulse facilitation (PPF), a form of short-term synaptic plasticity, was slightly elevated in Sca7$^{266Q/5Q}$ mice, with the greatest difference at 30 ms interpulse interval (Sca7$^{266Q/5Q}$, 158% ± 1%; WT, 135% ± 4%), but PPF across all interpulse intervals did not show statistically significant differences (Figure 8C).

Synaptic enhancement of the Shaffer collateral synapse following high-frequency stimulation (HFS) can be divided into three distinct phases: (1) initial LTP (I-LTP) (commonly referred to as short-term potentiation [STP]), (2) early LTP (E-LTP), and (3) late LTP (L-LTP) (Sweatt, 1999). Sca7$^{266Q/5Q}$ mice showed a significant reduction in I-LTP (indicated by the asterisk in Figure 8D), following the LTP-inducing HFS using a standard two trains of 100 Hz stimulation (Figure 8D), but normal E-LTP. We tested whether the same LTP impairment could be seen in Sca7$^{266Q/5Q}$ mice under the saturating HFS paradigm. LTP was induced in Sca7$^{266Q/5Q}$ mice with three pairings of 100 Hz stimulation (6×, 100 Hz trains total) (Figure 8E). This clearly shows that Sca7$^{266Q/5Q}$ mice are capable of maximum potentiation under saturating HFS. Consistent with our previous result, there was a significant reduction in I-LTP following the first pairing of stimulation, but the deficit in I-LTP could be rescued with successive pairings of 100 Hz stimulation (Figure 8E). A prominent component of I-LTP is posttetanic potentiation (PTP), a short-lived form of presynaptic plasticity immediately following HFS, characterized by greatly enhanced potentiation lasting for 1–5 min. In order to isolate the PTP component from I-LTP, the NMDA receptor antagonist 2-amino-5-phosphonovaleric acid (AP-5) was used to mask postsynaptic potentiation but leave PTP intact. Using this protocol, we found that the changes in I-LTP in Sca7$^{266Q/5Q}$ mice were due in part to a deficit in PTP (Figure 8F). We also tested NMDA receptor-independent LTP in Sca7$^{266Q/5Q}$ mice. Similar to the NMDA receptor-dependent LTP results, there was no difference in NMDA receptor-independent LTP between wild-type and Sca7$^{266Q/5Q}$ mice, and again a significant reduction in the first few minutes of LTP was observed (Figure 8G). Our data suggest that the I-LTP impairment in Sca7$^{266Q/5Q}$ mice is not restricted to stimulation in the 100 Hz frequency range, but is observed at higher stimulation frequencies (200 Hz) as well. Deficits in Sca7$^{266Q/5Q}$ I-LTP or PTP do not appear to be due to changes in baseline synaptic responses since EPSP wave forms from CA1 field recordings were indistinguishable from those of controls (Figure 8H).

We could not assess whether there was a behavioral correlate to this physiology because by 12 weeks of age the mutant mice were so deteriorated, and their vision so compromised, that it was impossible to ascertain which behaviors might be due to hippocampal dysfunction.

Discussion

To produce an authentic model for SCA7, we generated mice bearing a CAG repeat length that causes infantile-onset SCA7 in humans. Sca7$^{266Q/5Q}$ mice developed most of the salient features of the human disease. It is noteworthy that, although SCA7 is an autosomal dominant disease, Sca7$^{266Q/266Q}$ mice have a more accelerated phenotype than Sca7$^{266Q/5Q}$ mice, indicating a gene dosage effect. Homozygosity in SCA7 has never been reported, but homozygosity in other polyglutamine diseases such as MJD/SCA3, SCA6, and DRPLA advances the age of onset and increases disease severity (Kawakami et al., 1995; Lang et al., 1994; Sobue et al., 1996; Takiyama and Tsuji, 1995; Kato et al., 2000; Sato et al., 1995). Because expanded polyglutamine tracts lend deleterious properties to mutant proteins, higher levels of mutant proteins exacerbate the toxic effects.

Infantile SCA7 Clinical Phenotype

Expansions ranging from 200 to 460 CAG repeats invariably cause infantile-onset SCA7 in humans. Infantile

(C) Wild-type ataxin-7 is hardly detectable in WT retina, and NIs in Sca7$^{266Q/5Q}$ retina appear after the functional impairments. 1261 antibody did not detect wild-type ataxin-7 in WT retina. Mutant ataxin-7 staining, however, began to appear around 8 weeks of age as microggregates in Sca7$^{266Q/5Q}$ retina. Retinas of 12- and 18-week-old Sca7$^{266Q/5Q}$ mice shown reveal NIs in PE, ONL, INL, and GCL. The size and frequency of NIs increase as animal ages. NIs in INL is shown in insets (red boxes).
Scale bar indicates 50 μm. There is no difference among the 10-, 12-, 15-, and 18-week-old WT retina; therefore, only the retina from one stage is shown in (B) and (C) for WT.

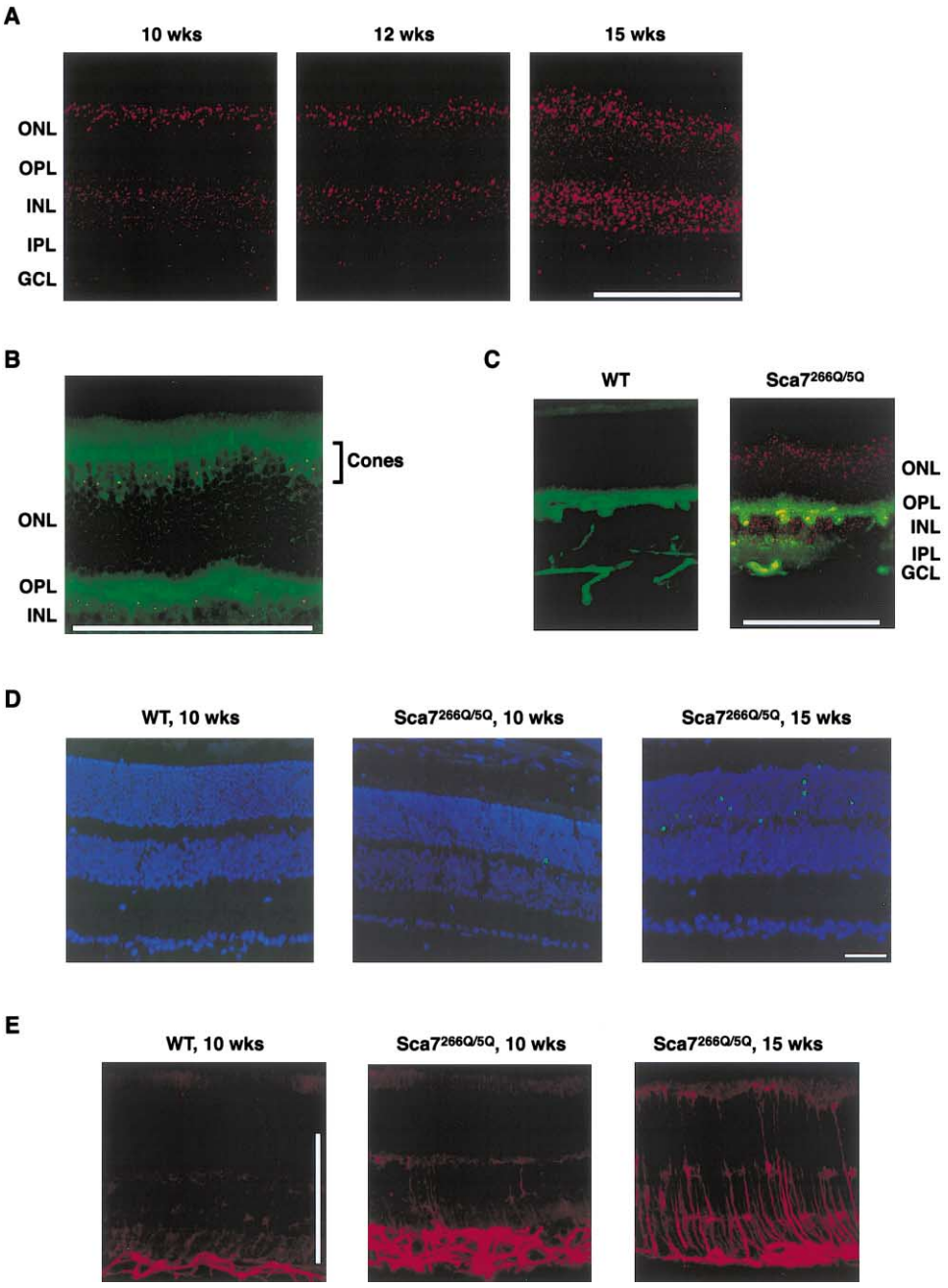

Figure 4. NIs and Apoptosis in Sca7$^{266Q/5Q}$ Retina

(A) NIs in Sca7$^{266Q/5Q}$ start predominantly in the top layer of ONL and throughout the INL. Immunofluorescence of 1261 antibody shows the distribution of NIs in Sca7$^{266Q/5Q}$ retina. The size and frequency of NIs increase over time.

(B) In ONL, the nuclei of cones are the ones where NIs develop first. Double labeling using 1261 antibody (red) and NSE antibody (green) shows the colocalization of mutant ataxin-7 and NSE in cones of 10-week-old Sca7$^{266Q/5Q}$ retina.

(C) NIs colocalize with horizontal cells and amacrine cells in INL. Double labeling using 1261 antibody (red) and calbindin antibody (green) shows NIs in horizontal cells and amacrine cells of retinas from 15-week-old mice. NIs are also observed in displaced amacrine cells in GCL.

(D) Apoptosis of photoreceptors occurs after photoreceptor dysfunction. TUNEL-positive signals (green) were found in ONL. Very few TUNEL-positive photoreceptors are seen at 10 weeks when ERG data indicate that there is a significant reduction in both cone and rod activities.

(E) Progressive activation of Müller glia in Sca7$^{266Q/5Q}$ retina. Retina sections were stained with GFAP antibody to demonstrate gliosis in Sca7$^{266Q/5Q}$ retina.

Scale bar indicates 50 μm. There is no difference between the 10- and 15-week-old WT retina; therefore, only the retina from one stage is shown in (D) and (E) for WT.

SCA7 not only shows an extremely rapid progression (children develop symptoms shortly after birth and die within 1–2 years), but the phenotype is much broader than that of adult-onset disease. In addition to ataxia, muscle wasting, kyphosis, ptosis, cone-rod dystrophy, and tremors, these infants can suffer from severe hypo-

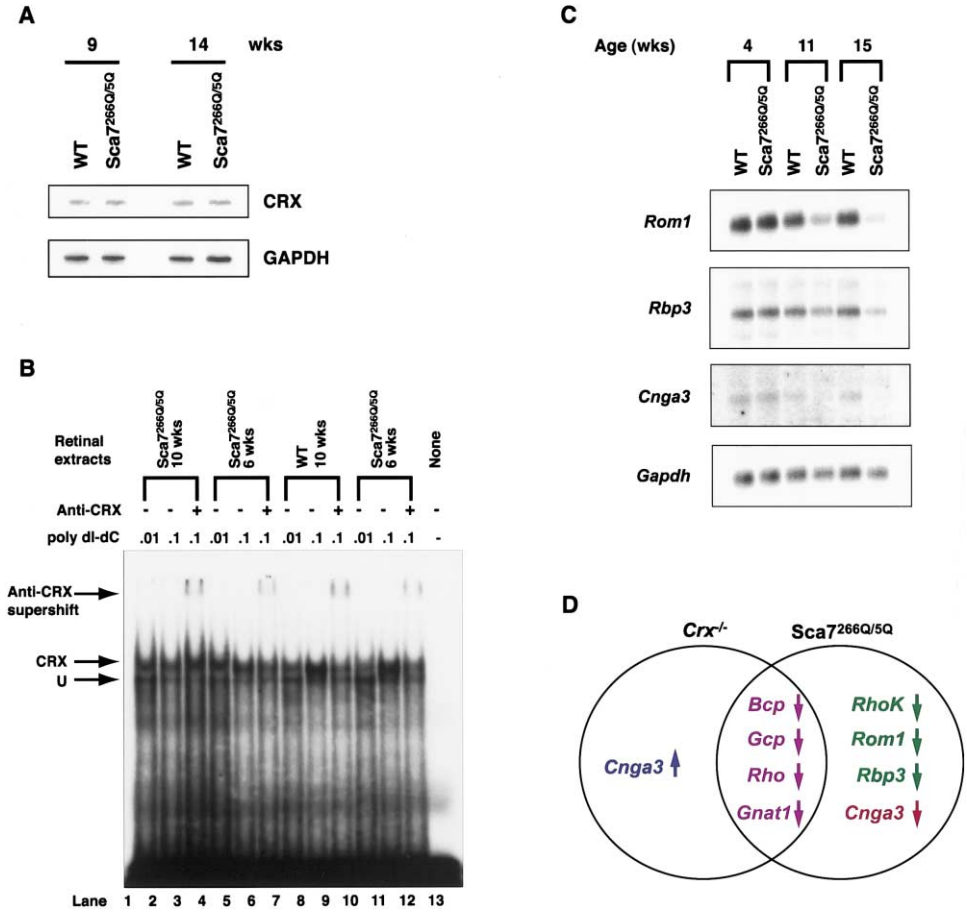

Figure 5. CRX and Retinal Dysfunction in Sca7$^{266Q/5Q}$ Mice

(A) CRX levels do not change in 9- and 14-week-old Sca7$^{266Q/5Q}$ retinas. Retinal protein extracts were prepared from 9- and 14-week-old mice. CRX antibody did not detect any difference in CRX level between WT and Sca7$^{266Q/5Q}$ mice. GAPDH antibody was used as a loading control.

(B) EMSAs for detecting DNA binding activity of CRX in the retina of WT and Sca7$^{266Q/5Q}$ mice show that CRX binding to Ret-4 is not altered in Sca7$^{266Q/5Q}$ retina. Ret-4 is known to be recognized by CRX and an unidentified ubiquitously expressed protein (U). Nuclear extracts were prepared from WT and Sca7$^{266Q/5Q}$ retinas at 6 and 10 weeks. 1.2 μg of retinal nuclear extracts were incubated with 1 nM of a ^{32}P-labeled Ret-4 probe in the presence of either 0.01 or 0.1 μg of poly dI-dC (Pharmacia). The binding activity of CRX was confirmed by the loss of the CRX band (labeled by an arrow), coinciding with the appearance of a supershift when 1 μl (0.5 μg) of the CRX antibody p261 (La Spada et al., 2001) was included in the EMSA reactions (lanes 3, 6, 9, and 12). The intensity of CRX-bound bands is similar between the WT and Sca7$^{266Q/5Q}$ lanes, indicating that there is no difference in CRX binding to its target site.

(C) Gene expression alterations in Sca7$^{266Q/5Q}$ mice. Genes that are not altered (*Rom1* and *Rbp3*) and a gene that is upregulated (*Cnga3*) in *Crx*$^{-/-}$ mice are all progressively downregulated in Sca7$^{266Q/5Q}$ retina.

(D) Venn diagram summarizing the patterns of photoreceptor-specific gene expression in *Crx*$^{-/-}$ and Sca7$^{266Q/5Q}$ mice. Genes that are downregulated in both mouse models are shown in purple. Direction of each arrow indicates increase (up arrow) and decrease (down arrow) in gene expression, respectively.

tonia, myoclonic seizures (Colan et al., 1981; Yoo and Zoghbi, 2002), and noncentral nervous system dysfunction such as congestive heart failure (Benton et al., 1998; Johansson et al., 1998; van de Warrenburg et al., 2001). Some autopsy studies show cerebellar atrophy and loss of Purkinje cells similar to those seen in adult SCA7 patients, but other infantile patients have grossly normal brains (Carpenter and Schumacher, 1966). Brainstem, spinal cord, and optic nerves appear normal in infantile cases, and the retinal pathology is confined to outer segment loss, leaving other areas of the retina intact (Ryan et al., 1975; de Jong et al., 1980; Traboulsi et al., 1988). Some infantile patients show loss of photoreceptors in the foveal and parafoveal areas of the ONL (Ryan et al., 1975; de Jong et al., 1980; Traboulsi et al., 1988). The limited cell loss in infantile cases is attributable to extremely short duration of the disease: neuronal dysfunction leads to demise before significant numbers of cells are lost.

The Sca7$^{266Q/5Q}$ Phenotype

Sca7$^{266Q/5Q}$ mice are strikingly similar in phenotype to an infant in the BASCA kindred who bore a similar number of CAG repeats (Benton et al., 1998). This infant showed symptom onset at about 1 month of age; Sca7$^{266Q/5Q}$ mice became distinguishable from their wild-type littermates (by showing motor incoordination) at 5 weeks. The signs of disease that developed in the knockin mouse paralleled features of this patient in kind and progression (see

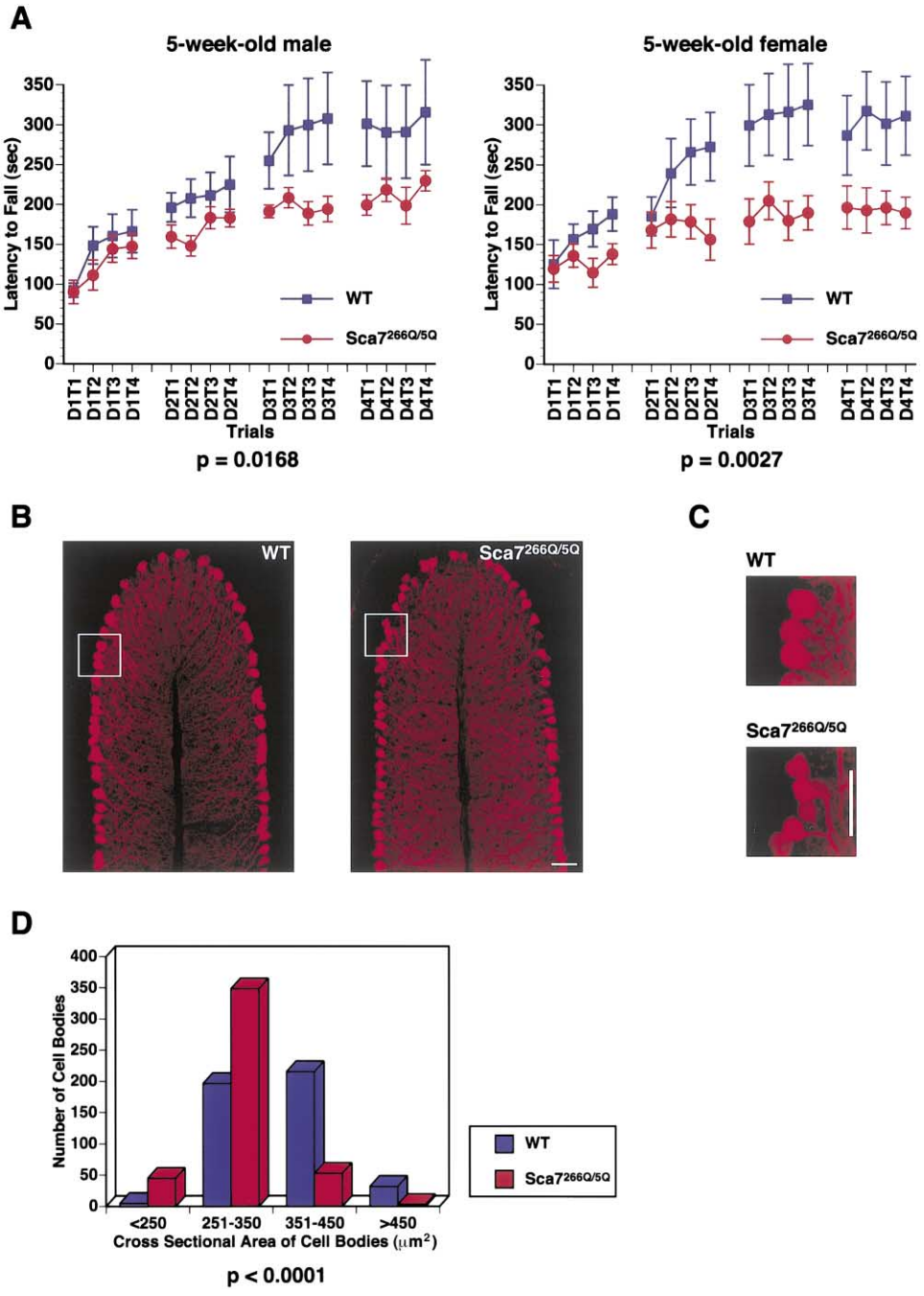

Figure 6. Sca7$^{266Q/5Q}$ Mice Show Impaired Rotarod Performance but No Purkinje Cell Loss

(A) 5-week-old male and female Sca7$^{266Q/5Q}$ mice have motor incoordination on a rotarod assay. 7 wild-type and 12 heterozygous male mice were tested, and 10 wild-type and 8 heterozygous female mice were tested.

(B) Confocal microscopy of anticalbindin-labeled Purkinje cells of 16-week-old Sca7$^{266Q/5Q}$ shows shrinkage of Purkinje cell bodies but no other distinct defects in mutant cerebellum. Scale bar = 50 μm.

(C) The boxed portions in (B) are magnified to better show the size difference of cell bodies. Scale bar = 50 μm.

(D) Purkinje cells from 16-week-old Sca7$^{266Q/5Q}$ mice have smaller cell bodies.

Table 1). Finally, some of the mutant mice developed myoclonic seizures, as do some infantile SCA7 patients.

The Sca7$^{266Q/5Q}$ mice thus show remarkable parallels to the human disease. It is also important to note that the pattern of cerebellar Purkinje cell degeneration in these mutants is quite distinct from that of SCA1 knockin mice (Watase et al., 2002): SCA1 knockin mice show reduced dendritic arborization of Purkinje cells, but the Sca7$^{266Q/5Q}$ mice, which have apparently normal dendritic arbors, have smaller than normal soma (Figures 6C and

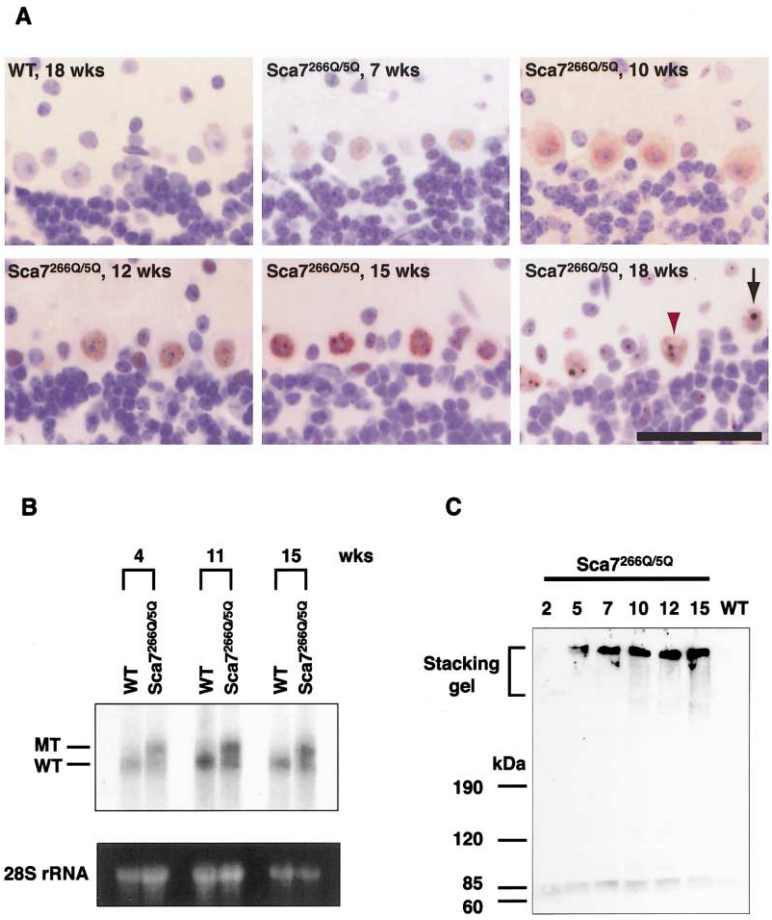

Figure 7. Progressive Accumulation of Mutant Ataxin-7 in Sca7$^{266Q/5Q}$ Mice

(A) Wild-type ataxin-7 is not detectable in wild-type cerebellum, but mutant ataxin-7 gradually accumulates in the nuclei of cerebellar Purkinje cells in Sca7$^{266Q/5Q}$ mice. Microaggregates are formed around 12 weeks of age. These aggregates later develop into single, large NIs. Black arrow and red arrowhead indicate NI and vacuole in Purkinje cells, respectively. Scale bar = 50 μm.

(B) The level of mutant *Sca7* transcript is not different from wild-type in Sca7$^{266Q/5Q}$ brain. Total RNA was prepared from mouse brain at indicated ages. 7.5 kb wild-type *Sca7* transcript is detected in both wild-type and Sca7$^{266Q/5Q}$ mice. 8.3 kb mutant *Sca7* transcript is detected only in Sca7$^{266Q/5Q}$ lanes.

(C) Mutant ataxin-7 is detected only in the stacking gel. 1261 antibody detected both wild-type ataxin-7 and mutant ataxin-7. The amount of mutant ataxin-7 in stacking gel increases over time.

6D). This difference points to the importance of protein context for determining specific aspects of the phenotype.

Retinal Dysfunction in Sca7$^{266Q/5Q}$ Mice

ERG studies of SCA7 patients show that cone dysfunction occurs prior to rod dysfunction, and both cone- and rod-driven ERGs gradually decrease with age (de Jong et al., 1980; Colan et al., 1981; Neetens et al., 1990; To et al., 1992). Sca7$^{266Q/5Q}$ mice undergo normal retinal development, but with increasing age beyond 5 weeks, they manifest ptosis and visual impairment. Our ERG data showed that cone dysfunction preceded rod dysfunction in these mutants, and M cones were affected before S cones (Figure 2). Northern analyses paralleled the ERG data in that the cone-specific markers were downregulated before the rod-specific markers, and *Gcp* downregulation occurred faster than *Bcp* (Figure 3A).

Like infantile SCA7 patients, Sca7$^{266Q/5Q}$ mice showed progressive shortening of the outer segments (Figure 3B). The outer segments are delicate structures containing proteins involved in the phototransduction cascade which are continuously renewed as the discs at the distal end are shed and phagocytosed by retinal pigment epithelial cells (Morrow et al., 1998; Pierce, 2001). Degeneration of outer segments results in blindness (Morrow et al., 1998). Mice with a targeted deletion of *Rho* showed a similar pattern of outer segment shortening and loss of rod photoreceptor activity (Humphries et al., 1997). Thus, shortening of outer segments in Sca7$^{266Q/5Q}$ mice might be attributable to the downregulation of photoreceptor-specific genes such as three photopigments (*Bcp*, *Gcp*, and *Rho*) and structural components of outer segments such as *Rom1* and *Prph2* (coding for Peripherin) (Figures 3A and 5C; data not shown).

It is interesting that although our ERG results parallel those of the groups that generated SCA7 transgenic mice (Yvert et al., 2000; La Spada et al., 2001), the pathology of the transgenics is markedly worse: their ONL becomes disorganized as they age, forming a "wavy" pattern. The transgenics also show significant photoreceptor loss. In contrast, Sca7$^{266Q/5Q}$ mice did not show much cell loss in the ONL (Figure 3B); apoptosis began around 10 weeks of age (Figure 4D), but these mutants retained more than 80% of the photoreceptors until the terminal stage of the disease. Loss of outer segments will eventually lead to the death of photoreceptors, but the short life span of the Sca7$^{266Q/5Q}$ mice precluded a significant loss of cells in either the retina or the cerebellum, much like the infantile SCA7 patients. Clearly, outer segment loss and altered gene expression are the earliest pathogenic events.

We were intrigued by the idea that CRX dysfunction may be responsible for cone-rod dystrophy in SCA7 (La Spada et al., 2001). Transcription of *Bcp*, *Gcp*, *Rho*, and

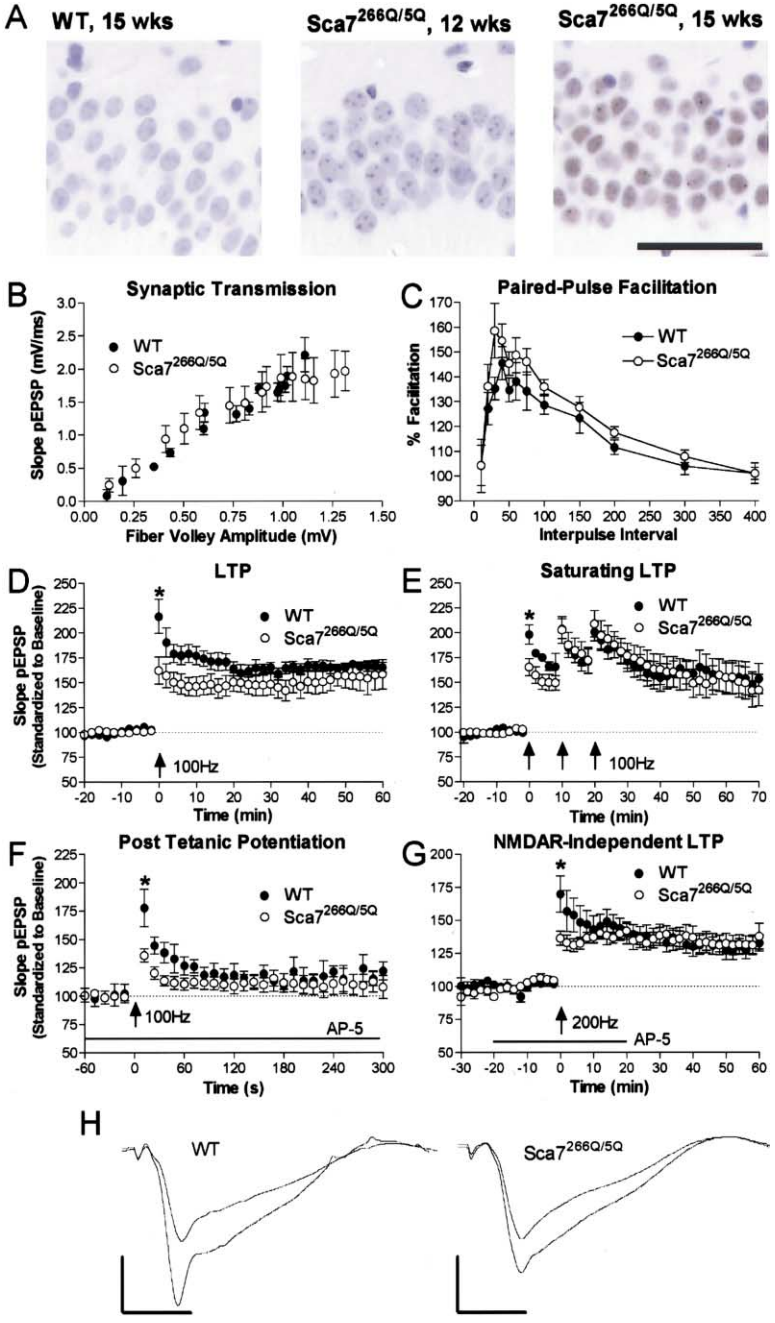

Figure 8. Reduced PTP in Sca7$^{266Q/5Q}$ Mice

(A) Wild-type ataxin-7 is barely detectable in wild-type hippocampus. Mutant ataxin-7 accumulates in nuclei of hippocampal CA1 pyramidal neurons and starts to form a punctate staining around 12 weeks of age, and the size and frequency of NIs increase with age.

(B) Sca7$^{266Q/5Q}$ mice show normal baseline synaptic transmission in the stratum radiatum of the CA1 region of the hippocampus, measured at 30°C (n = 7 for wild-type and mutant animals).

(C) Short-term plasticity assessed by PPF is unaffected in Sca7$^{266Q/5Q}$ mice.

(D) Sca7$^{266Q/5Q}$ hippocampal slices show reduced PTP (Sca7$^{266Q/5Q}$, 162% ± 13.4%, n = 10; WT, 216% ± 17.1%, n = 10; p = 0.022), but normal LTP induction 60 min posttetanus (Sca7$^{266Q/5Q}$, 158% ± 14.8%; WT 165% ± 4.5%) when induced with a standard HFS protocol consisting of two trains of a 1 s long, 100 Hz stimulation.

(E) PTP in Sca7$^{266Q/5Q}$ mice is rescued following the successive trains of 100 Hz stimulation. First train (Sca7$^{266Q/5Q}$, 165% ± 8.6%, n = 11; WT, 198.2% ± 9.6%, n = 6; p = 0.045). Second train (Sca7$^{266Q/5Q}$, 202% ± 13.2%; WT, 204% ± 10.1%). Third train (Sca7$^{266Q/5Q}$, 209% ± 13.4%; WT, 201% ± 9.1%).

(F) A closer examination of PTP was performed using a single train of 100 Hz stimulation in the presence of the NMDA receptor antagonist AP-5 (application is represented with a black bar), and pEPSPs were recorded every 12 s. Sca7$^{266Q/5Q}$ mice show a significant reduction in PTP immediately following HFS (Sca7$^{266Q/5Q}$, 135% ± 5.7%, n = 7; WT, 178% ± 16.5%, n = 5; p = 0.02)

(G) NMDA receptor-independent LTP induced using one train of 200 Hz stimulation for 1 s in the presence of AP-5 (application is represented with a black bar) also shows reduced PTP (Sca7$^{266Q/5Q}$, 137% ± 5.4%, n = 10; WT, 170% ± 13.6%, n = 10; p = 0.036). Results are shown as mean ± SEM.

(H) Representative traces (mean of six averaged successive pEPSPs, scale bars represent 1mV and 10 ms) showing differences in baseline pEPSPs compared to pEPSPs during PTP (immediately following 100 Hz HFS).

Gnat1 are controlled by CRX (Furukawa et al., 1999), and we knew that these genes were all progressively downregulated in Sca7$^{266Q/5Q}$ mice—but *Rhok*, a gene that is not altered in *Crx*$^{-/-}$ mice, was also downregulated in Sca7$^{266Q/5Q}$ mice (Figure 3A). This led us to consider the possibility that other factor(s) might also be involved in the downregulation of photoreceptor-specific genes in the Sca7$^{266Q/5Q}$ retina. Further expression analysis of more photoreceptor-specific genes (Figures 5C and 5D) lent support for this hypothesis: genes that are either upregulated or unaltered in *Crx*$^{-/-}$ mice were all progressively downregulated in Sca7$^{266Q/5Q}$ mice. *Crx*$^{+/-}$ mice with only one functional *Crx* allele show delayed maturation of their photoreceptors as manifested by the abnormal ERGs (both cone and rod ERGs) at 4 weeks of age, which improve at 8 weeks and are normal by 6 months of age (Furukawa et al., 1999). Sca7$^{266Q/5Q}$ mice, on the other hand, had normal rod ERGs at 5 weeks, did *not* show any improvement of the retinal function with age, but rather a deterioration over time (Table 2; Figure 2). In addition, *Crx*$^{+/-}$ mice do not show the same type of dysregulation of photoreceptor-specific genes observed in Sca7$^{266Q/5Q}$ mice; although downregulation of *Bcp* was observed in *Crx*$^{+/-}$ mice, *Gcp* was upregulated (Furukawa et al., 1999). The difference in the retinal phenotypes of Sca7$^{266Q/5Q}$ mice and *Crx* haploinsufficient mice argue that a simple model proposing that polyglutamine expansion in ataxin-7 reduces CRX activity by 2-fold or less is excluded.

CRX protein levels did not change in Sca7$^{266Q/5Q}$ retina

up to 14 weeks (Figure 5A), when the retinal dysfunction was pronounced. Moreover, CRX did not colocalize with NIs in Sca7$^{266Q/5Q}$ retina (data not shown). Because protein activity can change without any alteration in levels, we investigated the activity of CRX using EMSAs (Figure 5B). CRX binding to Ret-4 did not differ from wild-type in Sca7$^{266Q/5Q}$ retina at 3–7, 10, and 12 weeks. Lastly, it is of note that while there is overlap in the alterations seen in Sca7$^{266Q/5Q}$ mice and *Crx* null mice, there are some differences (Figure 5D). *Cnga3* typically upregulated in the *Crx* null mutants is downregulated in Sca7$^{266Q/5Q}$ mice; *Rhok*, *Rom1*, and *Rbp3* which are spared in *Crx* nulls are also downregulated in Sca7$^{266Q/5Q}$ mice. Although we cannot rule out the possible alteration of CRX transactivation in Sca7$^{266Q/5Q}$ retina, our data suggest that CRX dysfunction might not be the primary and/or only cause of retinal degeneration in SCA7. The compromise in CRX activity observed in SCA7 transgenic mice (La Spada et al., 2001) is probably brought out by the massive overexpression of the *SCA7* transgene from a heterologous promoter. Similar results have been observed in SCA1 mouse models: in SCA1 transgenic mice, downregulation of prenylcysteine carboxylnethyltransferase gene (*Pccmt*) occurred at postnatal day 11 (Lin et al., 2000), whereas it occurred after the onset of cerebellar dysfunction in SCA1 knockin mice (K. Watase and H.Y.Z., unpublished data). The data from these models indicate that the early molecular changes in transgenics might not accurately reflect what occurs in patients.

What mechanism, then, underlies the retinal dysfunction in Sca7$^{266Q/5Q}$ mice? We propose that the accumulation of mutant ataxin-7 results in progressive downregulation of photoreceptor-specific genes, leading to the structural disorganization of outer segments, and thus, to retinal dysfunction in Sca7$^{266Q/5Q}$ mice. It is noteworthy that accumulation of mutant ataxin-7 in Sca7$^{266Q/5Q}$ retina started in the cones and interneurons, spreading over to rods and ganglion cells later. Exactly how accumulated mutant ataxin-7 leads to downregulation of photoreceptor-specific genes is not exactly determined yet. The finding that several photoreceptor genes are downregulated in Sca7$^{266Q/5Q}$ mice raises the possibility that ataxin-7 acts as a corepressor. Alternatively, mutant ataxin-7 might interfere with the activity of one or more transcriptional coactivators in the retina.

Polyglutamine Expansion Does Indeed Impede Mutant Protein Degradation In Vivo

Although the wild-type *Sca7* transcript was abundantly expressed in mouse brain (Figure 7B), the level of wild-type ataxin-7 was very low (Figures 1C, 7A, 7C, and 8A). Wild-type ataxin-7 may be rapidly turned over in vivo. Mutant ataxin-7, on the other hand, progressively accumulated in various neurons in Sca7$^{266Q/5Q}$ brain and retina (Figures 3C, 4A, 7A, 7C, and 8A). The level of wild-type ataxin-7 may need to be maintained at low levels in order to tightly control its activity in these cells. The polyglutamine expansion seems to stabilize the mutant protein, slowing down its turnover rate and causing downstream molecular events that hinder cell function and survival. Mauger et al. have, in fact, shown that the level of wild-type ataxin-7 is too low to be detected with their CM189 antibody in control tissues, while the same antibody detected intense immunoreactivity as NIs in tissues of an early juvenile-onset SCA7 patient (Mauger et al., 1999). Likewise, Yvert et al. could not detect wild-type ataxin-7 in their SCA7 transgenic mice, but had no trouble detecting mutant ataxin-7 using the same promoter (Yvert et al., 2001).

Mutant ataxin-7 accumulated ubiquitously in various neuronal subtypes in the brain and retina as Sca7$^{266Q/5Q}$ mice aged; however, the speed of accumulation varied. Neurons in affected areas showed much more rapid accumulation of mutant protein than the ones in areas that are not obviously affected by disease. NIs developed in neurons only after sufficient amount of mutant protein was accumulated, and functional impairments became manifest. Thus, as in SCA1 knockin mice (Watase et al., 2002), the NIs are unlikely to initiate neuronal dysfunction. Indeed, NIs did not develop in the retina of Sca7$^{266Q/5Q}$ mice until after gene downregulation occurred. This is not to say that NIs, once present, may not further stimulate the degeneration already in progress; rather, it seems that it is the amount of mutant protein rather than the presence of NIs per se that is critical to cellular viability in SCA7 (the protein is no doubt accumulating in affected neurons before NIs become apparent). We propose that certain neuronal groups might have higher levels of proteins involved in refolding or degrading mutant ataxin-7. Such differences would explain the selective neuronal vulnerability that characterizes SCA7 and other polyglutamine diseases. Once NIs developed in neurons, they were subsequently tagged by ubiquitin and Hsc70 (Table 3). This suggests that, in addition to ataxin-7 accumulation, impaired clearance of ubiquitinated proteins (ataxin-7 and perhaps other proteins) forms another layer of events late in this pathogenic cascade. This may explain why late-stage disease, after ubiquitinated NIs appear, is associated with very rapid deterioration: once the clearance system is overwhelmed by accumulating protein, the additive effects take over quickly.

Effects of Mutant Ataxin-7 on Short-Term Synaptic Plasticity

The impairment in short-term synaptic plasticity in Sca7$^{266Q/5Q}$ mice is intriguing in that it is restricted to PTP and the first few minutes of LTP. Although not much is known about the molecular events that underlie PTP, it is thought to be generated by a prolonged rise in presynaptic $[Ca^{2+}]_i$ following HFS (Zucker and Regehr, 2002). HD knockin mice show a PTP reduction as well, but overall LTP and PPF are also decreased in these mice (Usdin et al., 1999), suggesting that the PTP impairment in Sca7 $^{266Q/5Q}$ mice is not caused merely by the presence of an expanded polyglutamine tract. Rather, the expanded polyglutamine tract in the context of ataxin-7 triggers this selective effect on short-term synaptic plasticity, which could result either from a toxic gain-of-function of the mutant protein or from enhancement of the endogenous function of ataxin-7 due to its stabilization. Further studies evaluating loss-of-function effects and molecular interactions of ataxin-7 should provide insight into the molecular basis of this phenotype.

Sca7$^{266Q/5Q}$ mice bear a CAG tract that has been reported in human patients and replicated the principle features of infantile SCA7 disease. Because the ex-

panded ataxin-7 was expressed in an accurate spatiotemporal pattern, we were able to pinpoint the early steps in pathogenesis. These mice will be valuable not only for exploring the mechanism of SCA7 and the efficacy of therapeutic interventions, but will also help unveil the mechanism of PTP alterations and their physiological significance.

Experimental Procedures

Generating Sca7$^{266Q/5Q}$ Mice

The 129/SvEv mouse genomic DNA library was screened using mouse EST clone W10624 (GenBank accession number), which is homologous to the 5′ end sequence of human *SCA7* exon 3. Two clones (named 6A and 17A) were pulled out from this screen and were used to construct a targeting vector. h*SCA7*.forward (5′-TTGTAGGAGCGGAAAGAATGTC-3′) and h*SCA7*.reverse (5′-ATCACT TCAGGACTGGGCAGAG-3′) were used to PCR amplify 306 CAG repeats and flanking regions from the published patient sample (Benton et al., 1998). 100 ng of patient genomic DNA was used in a 50 μl reaction tube containing 50 μM of each primer, 12.5% dimethylsulfoxide, 250 μM each dNTP, 1.5 mM $MgCl_2$, 50 mM KCl, 10 mM Tris-HCl (pH 8.3), and 4 U of *Taq* DNA polymerase. Cycling conditions were as follows: 95°C for 5 min followed by 35 cycles of denaturing at 94°C for 1 min, annealing at 62°C for 1 min, extension at 72°C for 2 min, and final extension at 72°C for 7 min. 198 bp NotI/HindIII fragment of mouse *Sca7* exon 3 was subcloned into pZErO 2.0 (Invitrogen). In order to introduce ApaI site in position 153, this clone was PCR amplified with M13 reverse primer and mSca7-ApaI primer (5′-GACGGCGGGCCCGGGGACACCACCACCTCG-3′). This changed 5′-GGCACC-3 into 5′-GGGCCC-3′ in position 150–155 of mouse *Sca7*. PCR product from the human patient sample was double digested with NotI and Bsp120I (isoschizomer of ApaI) and ligated into the mouse *Sca7* exon 3 with new ApaI site. Several subsequent ligation steps were followed to generate the *Sca7* knockin construct (19.8 kb). A selectable cassette containing the Neomycin resistance gene (*Neo*) and the Thymidine kinase gene (*Tk*) flanked by two *lox*P sites was inserted into the SacI site, which is about 2.3 kb downstream from exon 4. The 306 CAG repeats were highly unstable and contracted to 266 during the multiple ligation steps. *Sca7* knockin construct with 266 CAG repeats were electroporated into embryonic stem (ES) cells, and subsequent electroporation of Cre recombinase into the positive ES clones allowed the excision of *Neomycin* (*Neo*)/*Thymidine kinase* (*Tk*) selection cassette. Correctly targeted ES cells were injected into C57BL/6J blastocysts to generate chimeras, which were crossed to C57BL/6J females to obtain Sca7$^{266Q/5Q}$ mice. Germline transmission of a targeted allele was confirmed using both tail DNA Southern analyses and PCR amplification of CAG repeats. PCR conditions were same as above, and h*SCA7*.forward and m*Sca7*.hybrid.reverse (5′-CCACCC ACAGATTCCACGAC-3′) were used as primers.

Western Blot

Nuclear and cytoplasmic extracts of mouse cerebellum were obtained using NE-PER Nuclear And Cytoplasmic Extraction Reagents (Pierce). 100 μg of protein was loaded on 6% SDS gel. Dilution factor for 1261 was 1:1000. For expression analyses of CRX, retinal protein extracts were prepared by homogenizing mouse retinas in buffer containing 100 mM Tris (pH 6.8), 25 mM DTT, 2% SDS, and 2× complete protease inhibitor cocktail (Roche). 20 μg of extracts were loaded on 10% SDS gel. Dilution factor for CRX antibody was 1:500.

Electroretinograms (ERGs)

Flashes for scotopic measurements were generated by a Grass PS-33+ photostimulator. Light was spectrally filtered with a 500 nm interference filter (Edmund Scientific). A series of metal plates with holes of varying diameters and glass neutral density filters were used to attenuate the flash. As the intensity of the flash increased, the number of trials was decreased and the time between each flash was increased. To remove oscillatory potentials prior to fitting, the scotopic b-wave was digitally filtered using the filtfilt function in Matlab (low pass filter, $F_c = 60$ Hz). To calculate $b_{max,scot}$ and $I_{0.5}$, the peak value of each curve was fit to a saturating hyperbolic function (Naka-Rushton). For analysis of the a-wave and cone function, 1500 W Novatron xenon flash lamps provided intense illumination. To analyze the rod function, we used the following equation (Lamb-Pugh model) to fit a series of a-waves at increasing intensities:

$$1 - \frac{a(t)}{a_{max}} = \exp\left[-\frac{1}{2} \cdot \phi \cdot A \cdot (t - t_{eff})^2\right], \quad (1)$$

where $a(t)$ is the a-wave, a_{max} is its saturating amplitude, ϕ is the number of photoisomerizations rod produced by the flash, A is amplification factor, and t_{eff} is a brief delay. Because pathological studies indicated that the outer segments were shorter in Sca7$^{266Q/5Q}$ mice (Figure 3B), we substituted $\phi = I \cdot k$ into the equation, and fit for the parameter kA (Hood and Birch, 1994). I is intensity in scotopic cd/m^2 and k is variable with units ϕ/scotopic cd/m^2. Cone-driven responses were recorded using the paired flash technique. The first flash drove the rods temporarily into saturation. The second flash, delivered 2.5 s later, allowed the cones to recover, but not the rods. To isolate responses from S cones or M cones, we used bandpass interference filters centered at 365 and 500 nm (Edmund Scientific), respectively. To remove oscillatory potentials prior to fitting, the cone b-wave was digitally filtered using the filtfilt function in Matlab (low-pass filter, $F_c = 30$ Hz).

Northern Blots

Total RNA was isolated from the mouse eyes and brain with TRIZOL reagent following manufacture's instructions (Invitrogen). For expression analyses of photoreceptor-specific genes, 10 μg of total RNA from eyes was loaded on each lane for electrophoresis and transferred onto Hybond N+ nylon membrane (Amersham). All probes were obtained from the mouse EST clones (ATCC): *Bcp* (GenBank accession number BG293946, 295–818 bp PstI/NheI fragment), *Gcp* (GenBank accession number BG297657, 11–629 bp NcoI/KpnI fragment), *Rho* (GenBank accession number BG296640, 73–423 bp XhoI fragment), *Gnat1* (GenBank accession number BG404720, 68–646 bp BstXI/BamHI fragment), *Rhok* (GenBank accession number BG296640, 842–1387 bp KpnI/EcoRV fragment), *Rom1* (GenBank accession number BG404693, 9–515 bp NarI fragment), *Rbp3* (GenBank accession number BI737899, 846–1200 bp ApaI/BamHI fragment), and *Cnga3* (GenBank accession number BI730059, 537–1364 bp, SmaI fragment). For *Sca7* expression analyses, 15 μg of total RNA from brain was loaded on each lane for electrophoresis and transferred onto Hybond N+ nylon membrane (Amersham). Probe was isolated from mouse *Sca7* cDNA (360–912 bp HindIII/PstI fragment). Probes were labeled using Megaprime kit (Amersham) and hybridized in ExpressHyb hybridization solution (Clontech) according to manufacture's instructions. We measured the intensity of each band by densitometry.

Counting of the Number of Nuclei in the Vertical Length of ONL

Eyes of three mice were used for each genotype (five sections from the center/mouse). Sections were cut in 5 μm thickness. Pictures were taken at 20× magnification using a Zeiss Axioplan 2 fluorescence microscope and Axiocam camera following Hematoxylin and eosin staining. The number of vertical nuclei in ONL was counted every 25 μm on these pictures (five to six counts were performed/picture). Mean, SEM, and t test (two sample assuming unequal variance) were determined in Microsoft Excel.

TUNEL Staining

Eyes were fixed in 4% PFA/PBS for overnight at room temperature and cryoprotected by infiltrating from 15% sucrose/PBS to 30% sucrose/OCT (Tissue-Tek). They were subsequently embedded in OCT and cut as 10 μm sections onto Superfrost/Plus slides (Fisher Scientific). TUNEL assays were performed using In situ cell death detection kit, AP following manufacture's protocol (Roche). Images were acquired by a Zeiss Axioplan 2 fluorescence microscope and Axiocam camera.

Immunohistochemistry and Immunofluorescence

Immunohistochemical and immunofluorescent stainings were performed as previously described (Skinner et al., 1997; Cummings et

al., 1999; Pennesi et al., 2003). Antibodies used: 1261 (1:200), mouse monoclonal Calbindin (Sigma, 1:1000), mouse monoclonal NSE (Chemicon International, Inc., 1:200), rabbit polyclonal GFAP (Novus Biologicals, 1:1000), mouse monoclonal Hsp70/Hsc70 (StressGen, 1:200), mouse monoclonal Hsp70 (StressGen, 1:200), rabbit polyclonal Ubiquitin (StressGen, 1:300), mouse monoclonal CBP (Santa Cruz, 1:200), mouse monoclonal TBP (QED Bioscience Inc., 1:1000), and rabbit polyclonal TFIID (TBP) (Santa Cruz, 1:1000).

Purkinje Cell Counting

Brains of three mice were used for each genotype. Purkinje cells on three to six serial midsagittal cerebella hemisphere 5 μm sections (multiple sections/brain) were counted following Hematoxylin and eosin staining. Mean, SEM, and t test (two sample assuming equal variance) were determined in Microsoft Excel.

Quantifying Cell Body Size of Purkinje Cells

15 μm stacks of cerebellar optical sections were collected using a Zeiss 510 confocal microscope and averaged using the z projection function of NIH Image J. From three projected stacks (150 cells each) for each of three wild-type and three $Sca7^{266Q/5Q}$ mice, a total of 450 wild-type and 450 $Sca7^{266Q/5Q}$ cells were outlined manually and the cross-sectional area measured. Partial cells and binary cell images were excluded based upon cell shape and relative fluorescence intensity. Perikaryon area was estimated to be the approximately circular area enclosed by the cell perimeter and the extension of the cell perimeter toward the initial point of dendrite extension.

Electrophoretic Mobility Shift Assays (EMSAs)

Electrophoretic mobility shift assays were carried out as previously described (Chen et al., 1997) using mouse retinal nuclear extracts and a ^{32}P-labeled probe containing Ret-4, a CRX binding site from the bovine rhodopsin promoter.

Hippocampal Slice Preparation and Electrophysiology

Hippocampal slice preparation and electrophysiology were performed as previously described (Roberson and Sweatt, 1996). Briefly, hippocampal slices (400 μm) were maintained in an interface chamber and bathed in oxygenated artificial cerebral spinal fluid (ACSF, 125 mM NaCl, 2.5 mM KCl, 1.24 mM NaH_2PO_4, 25 mM $NaHCO_3$, 10 mM D-glucose, 2 mM $CaCl_2$ and 1 mM $MgCl_2$) (1 ml/min) at 30°C. Extracellular field recordings were made every 20 s in area CA1 stratum radiatum during stimulation of the Schaffer collateral pathway. Stable baseline synaptic transmission was established for 20 min at an intensity of 40%–50% of the maximum population excitatory postsynaptic potential (pEPSP) prior to LTP-inducing high-frequency stimulation (HFS). Stimulus intensity of the HFS was matched to the intensity used in the baseline recordings, and measurements are shown as the average slope of the pEPSP from six individual traces standardized to baseline recordings. LTP was induced by one or three sets of HFS, each set consisting of two trains of 100 Hz stimulation for 1 s, separated by 20 s (NMDA-dependent LTP induction), or a single train of 200 Hz stimulation for 1 s (NMDA-independent LTP induction). PTP was induced by a single 100 Hz HFS train for 1 s following at least 20 min of stable baseline recordings in the presence of AP-5. Immediately after the HFS, pEPSPs were recorded every 3 s for 5 min and are presented as the average of four individual traces.

Acknowledgments

We thank Barbara Antalffy and Zhuo Yang for technical assistance; Jean-Louis Mandel, Gäel Yvert, and Dominique Helmlinger for 1261 and 1597 antibodies; Monica Holmberg for SCA7 (1-135) antibody; and Vicky Brandt for a critical reading of the manuscript. This work was supported by the following NIH grants: NS27699 (to H.Y.Z.), EY12543 (to S.C.), EY 04446 and EY 02520 (to S.M.W.), and HD24064 (to the Baylor College of Medicine Mental Retardation Research Center). The Retina Research Foundation (Houston) and the International Retinal Research Foundation also support S.M.W. H.Y.Z is an Investigator with the Howard Hughes Medical Institute.

Received: July 12, 2002
Revised: December 17, 2002

References

Benton, C.S., de Silva, R., Rutledge, S.L., Bohlega, S., Ashizawa, T., and Zoghbi, H.Y. (1998). Molecular and clinical studies in SCA7 define a broad clinical spectrum and the infantile phenotype. Neurology *51*, 1081–1086.

Cancel, G., Duyckaerts, C., Holmberg, M., Zander, C., Yvert, G., Lebre, A.S., Ruberg, M., Faucheux, B., Agid, Y., Hirsch, E., et al. (2000). Distribution of ataxin-7 in normal human brain and retina. Brain *123*, 2519–2530.

Carpenter, S., and Schumacher, G.A. (1966). Familial infantile cerebellar atrophy associated with retinal degeneration. Arch. Neurol. *14*, 82–94.

Carter-Dawson, L.D., and LaVail, M.M. (1979). Rods and cones in the mouse retina. I. Structural analysis using light and electron microscopy. J. Comp. Neurol. *188*, 245–262.

Chen, S., and Zack, D.J. (1996). Ret-4, a positive acting rhodopsin regulatory element identified using a bovine retina *in vitro* transcription system. J. Biol. Chem. *271*, 28549–28557.

Chen, S., Wang, Q.L., Nie, Z., Sun, H., Lennon, G., Copeland, N.G., Gilbert, D.J., Jenkins, N.A., and Zack, D.J. (1997). Crx, a novel Otx-like paired-homeodomain protein, binds to and transactivates photoreceptor cell-specific genes. Neuron *19*, 1017–1030.

Colan, R.V., Snead, O.C., and Ceballos, R. (1981). Olivopontocerebellar atrophy in children: a report of seven cases in two families. Ann. Neurol. *10*, 355–363.

Cummings, C.J., Reinstein, E., Sun, Y., Antalffy, B., Jiang, Y., Ciechanover, A., Orr, H.T., Beaudet, A.L., and Zoghbi, H.Y. (1999). Mutation of the E6-AP ubiquitin ligase reduces nuclear inclusion frequency while accelerating polyglutamine-induced pathology in SCA1 mice. Neuron *24*, 879–892.

David, G., Abbas, N., Stevanin, G., Durr, A., Yvert, G., Cancel, G., Weber, C., Imbert, G., Saudou, F., Antoniou, E., et al. (1997). Cloning of the SCA7 gene reveals a highly unstable CAG repeat expansion. Nat. Genet. *17*, 65–70.

de Jong, P.T., de Jong, J.G., de Jong-Ten Doeschate, J.M., and Delleman, J.W. (1980). Olivopontocerebellar atrophy with visual disturbances. An ophthalmologic investigation into four generations. Ophthalmology *87*, 793–804.

de Raad, S., Szczesny, P.J., Munz, K., and Reme, C.E. (1996). Light damage in the rat retina: glial fibrillary acidic protein accumulates in Müller cells in correlation with photoreceptor damage. Ophthalmic Res. *28*, 99–107.

Fernandez-Funez, P., Nino-Rosales, M.L., de Gouyon, B., She, W.-C., Luchak, J.M., Martinez, P., Turiegano, E., Benito, J., Capovilla, M., Skinner, P.J., et al. (2000). Identification of genes that modify ataxin-1-induced neurodegeneration. Nature *408*, 101–106.

Furukawa, T., Morrow, E.M., Li, T., Davis, F.C., and Cepko, C.L. (1999). Retinopathy and attenuated circadian entrainment in *Crx*-deficient mice. Nat. Genet. *23*, 466–470.

Garden, G.A., Libby, R.T., Fu, Y.H., Kinoshita, Y., Huang, J., Possin, D.E., Smith, A.C., Martinez, R.A., Fine, G.C., Grote, S.K., et al. (2002). Polyglutamine-expanded ataxin-7 promotes non-cell-autonomous purkinje cell degeneration and displays proteolytic cleavage in ataxic transgenic mice. J. Neurosci. *22*, 4897–4905.

Goldberg, A.F., and Molday, R.S. (1996). Defective subunit assembly underlies a digenic form of retinitis pigmentosa linked to mutations in peripherin/rds and rom-1. Proc. Natl. Acad. Sci. USA *93*, 13726–13730.

Gusella, J.F., and MacDonald, M.E. (2000). Molecular genetics: unmasking polyglutamine triggers in neurodegenerative disease. Nat. Rev. Neurosci. *1*, 109–115.

Havener, W.H. (1951). Cerebellar-macular abiotrophy. Arch. Opthalmol. *25*, 40–43.

Hong, D.H., Pawlyk, B.S., Shang, J., Sandberg, M.A., Berson, E.L., and Li, T. (2000). A retinitis pigmentosa GTPase regulator (RPGR)-

deficient mouse model for X-linked retinitis pigmentosa (RP3). Proc. Natl. Acad. Sci. USA *97*, 3649–3654.

Hood, D.C., and Birch, D.G. (1994). Understanding changes in the b-wave of the ERG caused by heterogeneous receptor damage. Invest. Ophthalmol. Vis. Sci. *35*, 2948–2961.

Humphries, M.M., Rancourt, D., Farrar, G.J., Kenna, P., Hazel, M., Bush, R.A., Sieving, P.A., Sheils, D.M., McNally, N., Creighton, P., et al. (1997). Retinopathy induced in mice by targeted disruption of the rhodopsin gene. Nat. Genet. *2*, 216–219.

Johansson, J., Forsgren, L., Sandgren, O., Brice, A., Holmgren, G., and Holmberg, M. (1998). Expanded CAG repeats in Swedish spinocerebellar ataxia type 7 (SCA7) patients: effect of CAG repeat length on the clinical manifestation. Hum. Mol. Genet. *7*, 171–176.

Kato, T., Tanaka, F., Yamamoto, M., Yosida, E., Indo, T., Watanabe, H., Yoshiwara, T., Doyu, M., and Sobue, G. (2000). Sisters homozygous for the spinocerebellar ataxia type 6 (SCA6)/CACNA1A gene associated with different clinical phenotypes. Clin. Genet. *58*, 69–73.

Kawakami, H., Maruyama, H., Nakamura, S., Kawaguchi, Y., Kakizuka, A., Doyu, M., and Sobue, G. (1995). Unique features of the CAG repeats in Machado-Joseph disease. Nat. Genet. *9*, 344–345.

La Spada, A.R., Fu, Y.H., Sopher, B.L., Libby, R.T., Wang, X., Li, L.Y., Einum, D.D., Huang, J., Possin, D.E., Smith, A.C., et al. (2001). Polyglutamine-expanded ataxin-7 antagonizes CRX function and induces cone-rod dystrophy in a mouse model of SCA7. Neuron *31*, 913–927.

Lamb, T.D., and Pugh, E.N., Jr. (1992). G-protein cascades: gain and kinetics. Trends Neurosci. *15*, 291–298.

Lang, A.E., Rogaeva, E.A., Tsuda, T., Hutterer, J., and St George-Hyslop, P. (1994). Homozygous inheritance of the Machado-Joseph disease gene. Ann. Neurol. *36*, 443–447.

Lin, X., Antalffy, B., Kang, D., Orr, H.T., and Zoghbi, H.Y. (2000). Polyglutamine expansion down-regulates specific neuronal genes before pathologic changes in SCA1. Nat. Neurosci. *3*, 157–163.

Lin, C.H., Tallaksen-Greene, S., Chien, W.M., Cearley, J.A., Jackson, W.S., Crouse, A.B., Ren, S., Li, X.J., Albin, R.L., and Detloff, P.J. (2001). Neurological abnormalities in a knock-in mouse model of Huntington's disease. Hum. Mol. Genet. *10*, 137–144.

Lindenberg, K.S., Yvert, G., Muller, K., and Landwehrmeyer, G.B. (2000). Expression analysis of ataxin-7 mRNA and protein in human brain: evidence for a widespread distribution and focal protein accumulation. Brain Pathol. *10*, 385–394.

Lyubarsky, A.L., Falsini, B., Pennesi, M.E., Valentini, P., and Pugh, E.N., Jr. (1999). UV- and midwave-sensitive cone-driven retinal responses of the mouse: a possible phenotype for coexpression of cone photopigments. J. Neurosci. *19*, 442–455.

Lyubarsky, A.L., Chen, C., Simon, M.I., and Pugh, E.N., Jr. (2000). Mice lacking G-protein receptor kinase 1 have profoundly slowed recovery of cone-driven retinal responses. J. Neurosci. *20*, 2209–2217.

Mauger, C., Del-Favero, J., Ceuterick, C., Lubke, U., van Broeckhoven, C., and Martin, J. (1999). Identification and localization of ataxin-7 in brain and retina of a patient with cerebellar ataxia type II using anti-peptide antibody. Brain Res. Mol. Brain Res. *74*, 35–43.

Morrow, E.M., Furukawa, T., and Cepko, C.L. (1998). Vertebrate photoreceptor cell development and disease. Trends Cell Biol. *9*, 353–358.

Nakamura, K., Jeong, S.Y., Uchihara, T., Anno, M., Nagashima, K., Nagashima, T., Ikeda, S., Tsuji, S., and Kanazawa, I. (2001). SCA17, a novel autosomal dominant cerebellar ataxia caused by an expanded polyglutamine in TATA-binding protein. Hum. Mol. Genet. *10*, 1441–1448.

Neetens, A., Martin, J.J., Libert, J., and Van den Ende, P. (1990). Autosomal dominant cone dystrophy-cerebellar atrophy (ADCoCA) (modified ADCA Harding II). Neuroophthalmology *10*, 261–275.

Pennesi, M.E., Cho, J.H., Yang, Z., Wu, S., Zhang, J., Wu, S.M., and Tsai, M.J. (2003). BETA2/NeuroD null mice: a new model for transcription factor dependent photoreceptor degeneration. J. Neurosci., in press.

Pierce, E.A. (2001). Pathways to photoreceptor cell death in inherited retinal degenerations. Bioessays *23*, 605–618.

Pugh, E.N., Jr., Falsini, B., and Lyubarsky, A.L. (1998). The origin of the major rod- and cone-driven components of the rodent electroretinogram, and the effect of age and light-rearing history on the magnitudes of these components. In Photostasis and Related Topics, T.P. Williams and A.B. Thistle, eds. (New York: Plenum), pp. 93–128.

Rattner, A., Smallwood, P.M., Williams, J., Cooke, C., Savchenko, A., Lyubarsky, A., Pugh, E.N., and Nathans, J. (2001). A photoreceptor-specific cadherin is essential for the structural integrity of the outer segment and for photoreceptor survival. Neuron *32*, 775–786.

Rich, K.A., Zhan, Y., and Blanks, J.C. (1997). Migration and synaptogenesis of cone photoreceptors in the developing mouse retina. J. Comp. Neurol. *388*, 47–63.

Roberson, E.D., and Sweatt, J.D. (1996). Transient activation of cyclic AMP-dependent protein kinase during hippocampal long-term potentiation. J. Biol. Chem. *271*, 30436–30441.

Ryan, S.J.J., Knox, D.L., Green, W.R., and Konigsmark, B.W. (1975). Olivopontocerebellar degeneration. Clinicopathologic correlation of the associated retinopathy. Arch. Ophthalmol. *93*, 169–172.

Sato, K., Kashihara, K., Okada, S., Ikeuchi, T., Tsuji, S., Shomori, T., Morimoto, K., and Hayabara, T. (1995). Does homozygosity advance the onset of dentatorubral-pallidoluysian atrophy? Neurology *45*, 1934–1936.

Semple-Rowland, S.L., Adamus, G., Cohen, R.J., and Ulshafer, R.J. (1991). Expression of glial fibrillary acidic protein by Müller cells in rd chick retina. Electrophoresis *12*, 307–312.

Skinner, P.J., Koshy, B.T., Cummings, C.J., Klement, I.A., Helin, K., Servadio, A., Zoghbi, H.Y., and Orr, H.T. (1997). Ataxin-1 with an expanded glutamine tract alters nuclear matrix-associated structures. Nature *389*, 971–974.

Sobue, G., Doyu, M., Nakao, N., Shimada, N., Mitsuma, T., Maruyama, H., Kawakami, S., and Nakamura, S. (1996). Homozygosity for Machado-Joseph disease gene enhances phenotypic severity. J. Neurol. Neurosurg. Psychiatry *60*, 354–356.

Ström, A.L., Jonasson, J., Hart, P., Brannstrom, T., Forsgren, L., and Holmberg, M. (2002). Cloning and expression analysis of the murine homolog of the spinocerebellar ataxia type 7 (SCA7) gene. Gene *285*, 91–99.

Sweatt, J.D. (1999). Toward a molecular explanation for long-term potentiation. Learn. Mem. *6*, 399–416.

Takiyama, Y., and Tsuji, S. (1995). The characteristics and the gene locus of Machado Joseph disease. No To Shinkei *47*, 117–129.

To, K.W., Adamian, M., Jakobiec, F.A., and Berson, E.L. (1992). Olivopontocerebellar atrophy with retinal degeneration. An electroretinography and histopathologic investigation. Ophthalmology *100*, 15–23.

Traboulsi, E.I., Maumenee, I.H., Green, W.R., Freimer, M.L., and Moser, H. (1988). Olivopontocerebellar atrophy with retinal degeneration. A clinical and ocular histopathologic study. Arch. Ophthalmol. *106*, 801–806.

Usdin, M.T., Shelbourne, P.F., Myers, R.M., and Madison, D.V. (1999). Impaired synaptic plasticity in mice carrying the Huntington's disease mutation. Hum. Mol. Genet. *8*, 839–846.

van de Warrenburg, B.P., Frenken, C.W., Ausems, M.G., Kleefstra, T., Sinke, R.J., Knoers, N.V., and Kremer, H.P. (2001). Striking anticipation in spinocerebellar ataxia type 7: the infantile phenotype. J. Neurol. *248*, 911–914.

Watase, K., Weeber, E.J., Xu, B., Antalffy, B., Yuva-Paylor, L., Hashimoto, K., Kano, M., Atkinson, R., Sun, Y., Armstrong, D.L., et al. (2002). A long CAG repeat in the mouse *Sca1* locus replicates SCA1 features and reveals the impact of protein solubility on selective neurodegeneration. Neuron *34*, 905–919.

Yoo, S., and Zoghbi, H.Y. (2002). Dominantly inherited spinocerebellar syndromes. In Neuromuscular Disorders of Infancy, Childhood, and Adolescence: A Clinician's Approach, H.R. Jones, D.C. De Vivo, and B.T. Darras, eds. (Woburn, MA: Butterworth-Heinemann), pp. 1165–1183.

Yvert, G., Lindenberg, K.S., Picaud, S., Landwehrmeyer, G.B., Sahel, J.A., and Mandel, J.-L. (2000). Expanded polyglutamines induce neurodegeneration and trans-neuronal alterations in cerebellum and retina of SCA7 transgenic mice. Hum. Mol. Genet. *9*, 2491–2506.

Yvert, G., Lindenberg, K.S., Devys, D., Helmlinger, D., Landwehrmeyer, G.B., and Mandel, J.-L. (2001). SCA7 mouse models show selective stabilization of mutant ataxin-7 and similar cellular responses in different neuronal cell types. Hum. Mol. Genet. *10*, 1679–1692.

Zoghbi, H.Y., and Botas, J. (2002). Mouse and fly models of neurodegeneration. Trends Genet. *18*, 463–471.

Zoghbi, H.Y., and Orr, H.T. (2000). Glutamine repeats and neurodegeneration. Annu. Rev. Neurosci. *23*, 217–247.

Zucker, R.S., and Regehr, W.G. (2002). Short-term synaptic plasticity. Annu. Rev. Physiol. *64*, 355–405.